Journal of
Medicinal Chemistry

Article

Red-emitting dibenzodiazepinone derivatives as fluorescent dualsteric probes for the muscarinic acetylcholine M receptor

Xueke She, Andrea Pegoli, Corinna G. Gruber, David Wifling, Jessica Carpenter, Harald Hübner, Mengya Chen, Jianfei Wan, Günther Bernhardt, Peter Gmeiner, Nicholas D. Holliday, and Max Keller

J. Med. Chem., **Just Accepted Manuscript** • DOI: 10.1021/acs.jmedchem.9b02172 • Publication Date (Web): 01 Apr 2020

Just Accepted

is published by the American Chemical Society. 1155 Sixteenth Street N.W., Washington, DC 20036

Red-emitting dibenzodiazepinone derivatives as fluorescent dualsteric probes for the muscarinic acetylcholine M_2 receptor

Xueke She,[†,$,#] *Andrea Pegoli,*[†,€,#] *Corinna G. Gruber,*[†] *David Wifling,*[†,¥] *Jessica Carpenter,*[‡] *Harald Hübner,*[‖] *Mengya Chen,*[†,⊥] *Jianfei Wan,*[†,§] *Günther Bernhardt,*[†] *Peter Gmeiner,*[‖] *Nicholas D. Holliday*,*[‡] *and Max Keller*,*[†]

[†] *Institute of Pharmacy, Faculty of Chemistry and Pharmacy, University of Regensburg, Universitätsstr. 31, D-93053 Regensburg, Germany*

[‡] *School of Life Sciences, University of Nottingham, Queen's Medical Centre, Derby Road, Nottingham NG7 2UH, United Kingdom*

[‖] *Department of Chemistry and Pharmacy, Medicinal Chemistry, Friedrich Alexander University, Nikolaus-Fiebiger-Straße 10, D-91058 Erlangen, Germany*

ABSTRACT

Fluorescently labeled dibenzodiazepinone-type muscarinic acetylcholine receptor (MR) antagonists, including dimeric ligands, were prepared using red-emitting cyanine dyes. Probes containing a fluorophore with negative charge showed high M_2R affinities (pK_i (radioligand competition binding): 9.10-9.59). Binding studies at M_1 and M_3-M_5 receptors indicated a M_2R preference. Flow cytometric and high-content imaging saturation and competition binding (M_1R, M_2R and M_4R) confirmed occupation of the orthosteric site. Confocal microscopy revealed that fluorescence was located mainly at the cell membrane (CHO-hM_2R cells). Results from dissociation and saturation binding experiments (M_2R) in the presence of allosteric M_2R modulators (dissociation: W84, LY2119620 and alcuronium; saturation binding: W84) were consistent with a competitive mode of action between the fluorescent probes and the allosteric ligands. Taken together, these lines of evidence indicate that these ligands are useful fluorescent molecular tools to label the M_2R in imaging and binding studies, and suggest that they have a dualsteric mode of action.

Introduction

Fluorescence-based techniques have been increasingly used for studying ligand-receptor interactions, and hence there is a growing demand for suitable fluorescent receptor ligands. Compared with radiolabeled probes, fluorescent ligands are advantageous with respect to safety precautions and waste disposal. Moreover, they are applicable to fluorescence microscopy and flow cytometry, routine techniques in many laboratories, as well as to various homogeneous assay systems requiring specialized multimode plate readers,[1-3] such as high-content imaging based assays, or polarization based fluorescence anisotropy receptor binding studies.[4,5] A general issue regarding the design of small-molecule fluorescent ligands is the impairment of the bioactivity caused by conjugation to bulky fluorophores. For this reason, the pharmacophore (ligand) and the fluorophore are often held apart by a linker or spacer moiety.[6-8] There are numerous reports on fluorescent probes for GPCRs, for instance for neuropeptide Y,[9-14] histamine,[15-19] opioid,[20-22] dopamine,[23,24] neurotensin,[25-28] and adenosine[29] receptors. Concerning muscarinic acetylcholine receptors (MRs), several fluorescently labeled M_1R ligands, derived from the M_1 subtype preferring MR antagonist pirenzepine, were reported (for instance, compound **1**, Figure 1A).[30,31] Likewise, conjugation of the MR ligands tolterodine, telenzepine and AC-42 to fluorescent dyes resulted in probes with high to moderate M_1R affinity (compounds **2-4**, Figure 1A).[32-35] Compounds **1** and **4** were reported to bind bitopically/dualsterically to the hM_1R,[30,35] i.e. they bind simultaneously to the orthosteric and an allosteric site of the receptor. In contrast to the M_1R, reports on fluorescent probes for the M_2-M_5 receptor subtypes, characterized at cloned MRs, are rare: the non-selective fluorescent M_1R ligands **2** and **3** were reported to exhibit also high M_2-M_5 receptor and high M_2R affinity, respectively (Figure 1A),[33,36] and pyridinium-styryl-type fluorescent dyes were shown to bind to all MR subtypes at medium nanomolar concentrations.[37]

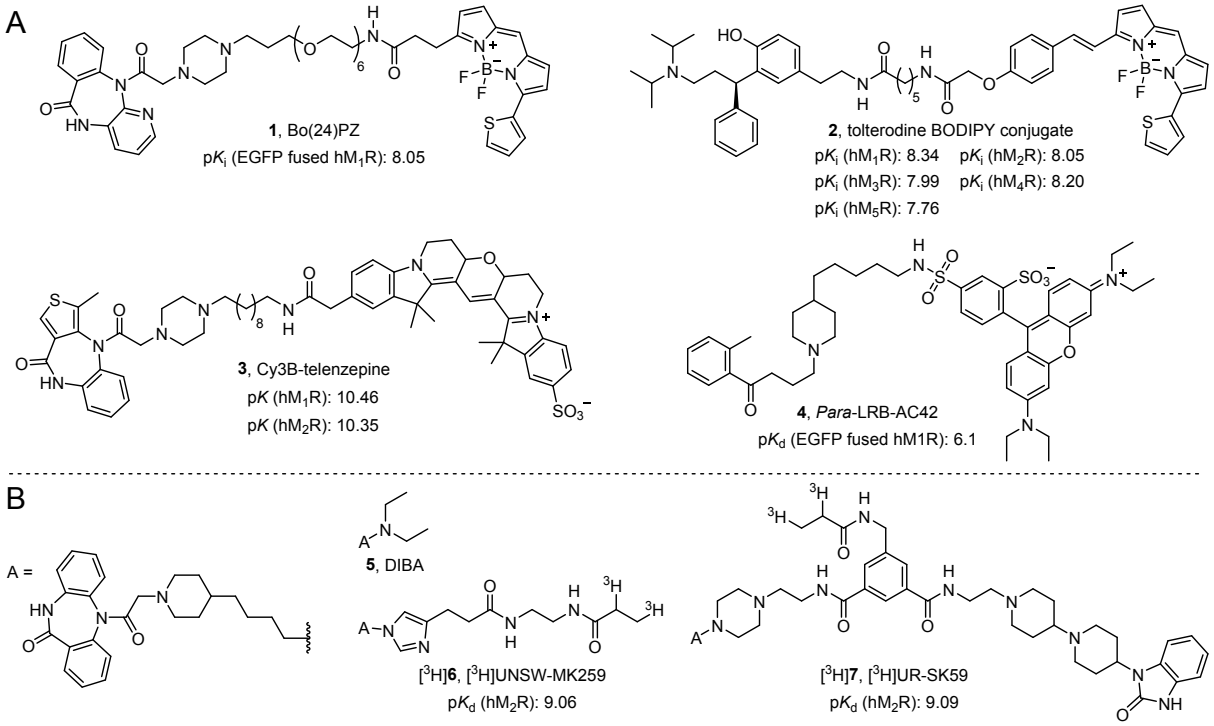

Figure 1. (A) Structures, M_1R affinities (and M_2R binding data, if available) of the reported fluorescently labeled M_1R ligands **1-4**[30,32-36] (in case of **1**[30] and **2**,[33] reported K_i values were converted to pK_i values). (B) Structures and M_2R affinities of the dibenzodiazepinone-type MR ligand DIBA and the DIBA-derived radioligands [^{3}H]UR-MK259 and [^{3}H]UR-SK59 (reported K_d values were transformed to pK_d values).[38,39]

Prompted by the recently reported synthesis and characterization of radiolabeled dualsteric M_2R antagonists derived from the M_2R preferring dibenzodiazepinone DIBA (**5**)[40] (for instance, [^{3}H]**6** and [^{3}H]**7**, Figure 1B),[38,39] exhibiting high M_2R affinity, we conjugated two types of red-emitting fluorophores to previously reported amine-functionalized dibenzodiazepinone derivatives.[38,39] This approach yielded twelve fluorescent MR ligands, which were studied with respect to their M_1R-M_5R affinities. Selected fluorescent ligands were characterized by flow cytometry and high-content imaging based binding studies as well as by confocal microscopy to investigate their applicability as molecular tools.

Results and Discussion

Chemistry. The fluorescent monomeric and dimeric dibenzodiazepinone-type MR ligands (**10**,[41] **12**,[41] **14**,[41] **16-18**,[41] **20**,[41] **22**, **23**, **27**, **28**, **30**) were prepared from previously reported amine-functionalized precursor compounds (**8**,[42] **15**,[39] **21**,[42] **26**,[38] **29**[39]) and the pyrylium dye **9** as well as the indolinium-type cyanine dye succinimidyl esters **11**, **13** and **19** (Scheme 1). The latter contain the same fluorophore core structure but differ with respect to attached sulfonic acid groups leading to different net charges of the dye (*cf.* Scheme 1 and Figure 2). Pyrylium dyes such as **9**, originally developed for the staining of proteins,[43] react readily with primary amines at pH > 8 to give the corresponding pyridinium adducts (pyridinium-type cyanine dyes), which exhibit a large Stokes' shift and can be excited with an argon laser (488 nm) (*cf.* Figure S2, Supporting Information).

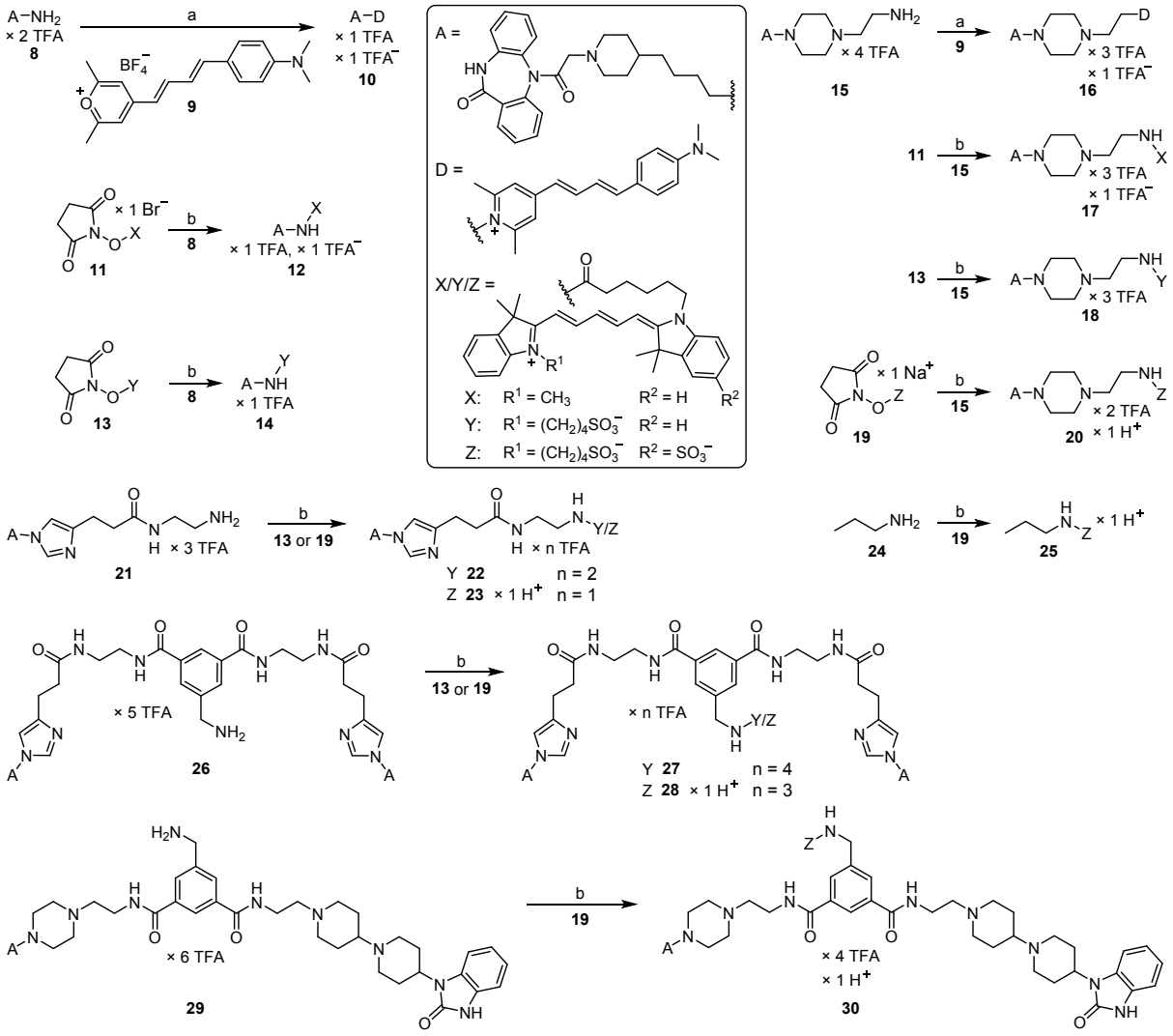

Scheme 1. Synthesis of the red-emitting dibenzodiazepinone-type MR ligands (structures also shown in Figure 2), containing a pyridinium-type (**10**, **16**) or an indolinium-type (**12**, **14**, **17**, **18**, **20**, **22**, **23**, **27**, **28**, **30**) cyanine fluorophore, and reference compound **25**. Reagents and conditions: (a) triethylamine, DMF, rt, 2 h, 21% (**10**), 34% (**16**); (b) DIPEA, DMF, rt, 1-2 h, 40% (**12**), 37% (**14**), 31% (**17**), 30% (**18**), 30% (**20**), 34% (**22**), 41% (**23**), 36% (**27**), 26% (**28**), 34% (**30**).

Treatment of the amine precursors **8** and **15** with **9** in the presence of triethylamine yielded the pyridinium-type fluorescent ligands **10** and **16**, respectively (Scheme 1). The cyanine labeled monomeric MR ligands **12**, **14**, **17**, **18**, **20**, **22** and **23** were prepared by acylation of amines **8**,

15 and **21** using the succinimidyl esters **11**, **13** or **19** (Scheme 1). Reference compound **25**[27] was obtained by treatment of propylamine (**24**) with succinimidyl ester **19**. The homodimeric fluorescent MR ligands **27** and **28** were synthesized from amine **26** and compounds **13** and **19**, respectively. Treatment of amine precursor **29**, containing the pharmacophore of **5** and pharmacophoric groups of TBPB, a compound described as an allosteric and bitopic M_1R ligand,[44-47] afforded the heterodimeric fluorescent MR ligand **30** (Scheme 1).

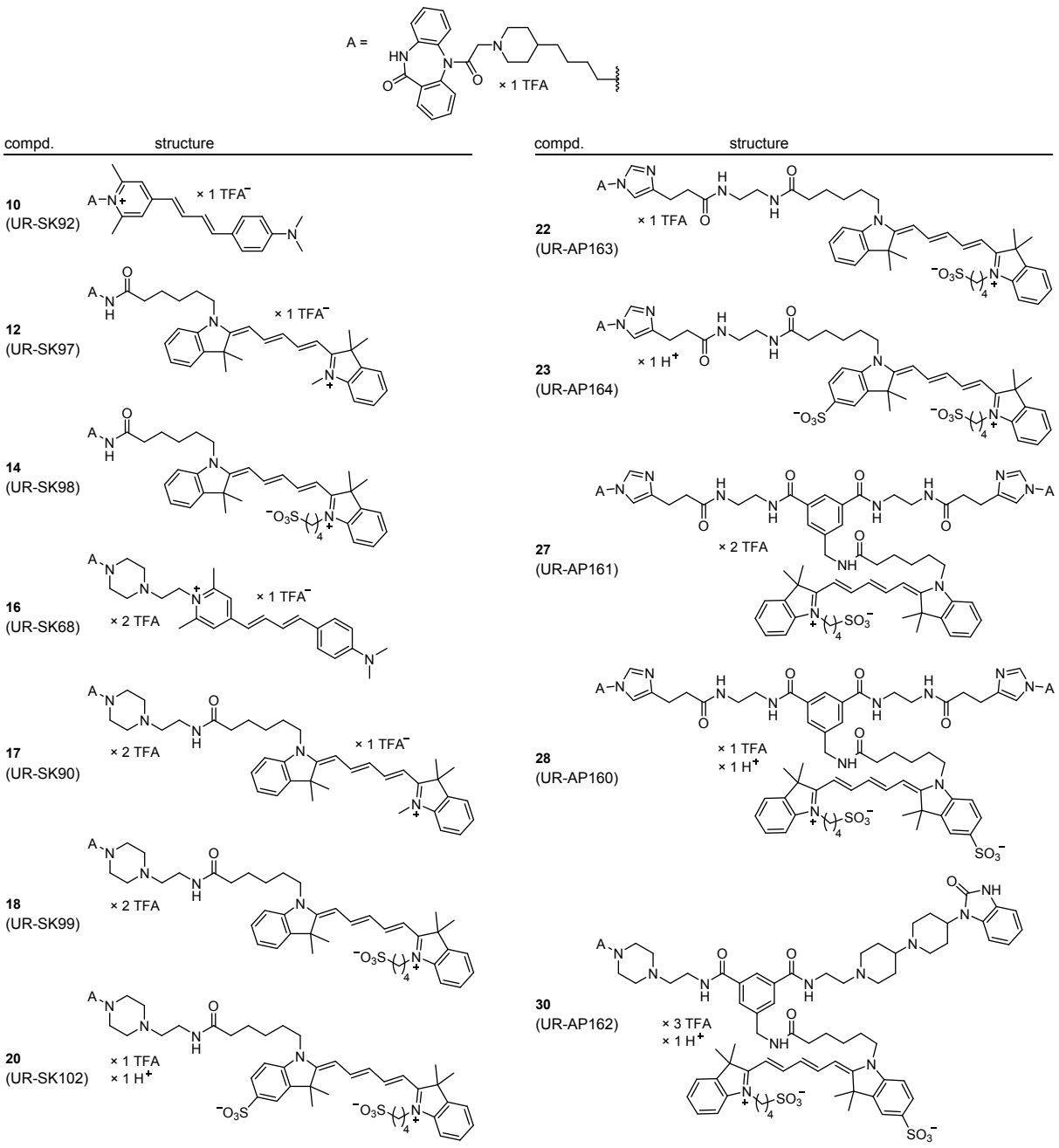

Figure 2. Structures of the synthesized and investigated fluorescent dibenzodiazepinone-type MR ligands.

The fluorescent ligands **20**, **23**, **28** and **30** were investigated with respect to their stability under assay-like conditions, i.e. in PBS pH 7.4. In all cases, no decomposition was observed by HPLC analysis within the incubation period of 48 h (Figure S1, Supporting Information). Interestingly, the vessel material (siliconized glass tube) strongly adsorbed compound **28**, resulting in a reduction of the peak area by approx. 90% after 24 h (Figure S1C, Supporting Information). Using other materials (polypropylene and "siliconized" polypropylene tubes) did not lower the adsorption of **28** (data not shown). Likewise, adsorption of **30** to the vessel material (polypropylene) resulted in a reduction of the peak area by approx. 50% (Figure S1D). Adsorption of **30** to a siliconized glass tube was comparable (data not shown). Notably, after removal of the aqueous solution after 48 h, most of **28** and **30** could be desorbed and recovered by rinsing of the tube with acetonitrile/0.1% aq TFA (1:1 v/v) (Figure S1C and S1D, Supporting Information).

Radioligand Competition Binding Studies with [^{3}H]NMS. M_1R-M_5R affinities of the fluorescently labeled dibenzodiazepinone derivatives (**10**, **12**, **14**, **16-18**, **20**, **22**, **23**, **27**, **28** and **30**) were determined at intact CHO-hM_xR cells (x = 1-5) using the orthosteric antagonist [^{3}H]NMS as radioligand (for competition binding curves see Figure S2, Supporting Information). The fluorescent ligands with the lowest M_2R affinities within this series of compounds (pK_i 6.85-8.52; Table 1) contained a fluorophore with positive (+1) net charge (**10**, **12**, **16**, **17**) or no net charge (**14**). Fluorescent ligands containing a fluorophore with negative (−1) net charge (**20**, **23**, **28**, **30**) exhibited the highest M_2R affinities (pK_i 9.10-9.59). These data suggest that the net charge of the fluorophore has an impact on the M_2R affinity, becoming obvious, in particular, in case of compounds **17**, **18** and **20**, which contain the same pharmacophore, linker and fluorophore core structure, but vary with respect to the fluorophore net charge (*cf*. Figure 2, Table 1). The complete MR selectivity profile was determined for fluorescent ligands **10**, **12**, **14**, **16-18**, **20**, **23**, **28** and **30** (Table 1). Whereas compounds **23** and

30 exhibited a modest preference for the M_2R over the M_1 and M_4 receptor, the other compounds proved to be rather non-selective with respect to M_1, M_2 and M_4 receptor binding (Table 1). A clear M_2R over M_3R and M_5R selectivity was observed for **16**, **18**, **20**, **23**, **28** and **30** (difference in pK_i > 1.5 log units). Some [^{3}H]NMS displacement curves revealed steep curve slopes (for instance, in case of compound **17** (M_2R): slope = −2.3), indicating a complex mechanism, e.g., an involvement of more than one binding site, receptor oligomerization or the existence of multiple conformational receptor states.[48-51]

Table 1. M_2 (and M_1, M_3-M_5) receptor affinities (pK_i values) of the fluorescent DIBA derivatives **10**, **12**, **14**, **16-18**, **20**, **22**, **23**, **27**, **28** and **30**, as well as of the precursor compounds **8**, **15**, **21**, **26** and **29** obtained from equilibrium competition binding studies with [^{3}H]NMS at live CHO-hM_xR cells (x = 1-5).[a]

compd.	M_1R		M_2R		M_3R		M_4R		M_5R	
	pK_i	slope[b]	pK_i	slope[b]	pK_i	slope[b]	pK_i	slope[b]	pK_i	slope[b]
8	-		7.97 ± 0.03[c]	−0.98 ± 0.07	-		-		-	
10	7.51 ± 0.07	−1.5 ± 0.2	7.77 ± 0.08	−1.2 ± 0.2	7.07 ± 0.06	−1.3 ± 0.1	7.79 ± 0.03	−1.3 ± 0.04[c]	6.70 ± 0.06	−1.6 ± 0.1[d]
12	6.92 ± 0.07	−1.3 ± 0.1	7.27 ± 0.04	−1.6 ± 0.2	6.20 ± 0.03	−1.7 ± 0.1[d]	7.17 ± 0.02	−1.4 ± 0.1	6.54 ± 0.09	−1.7 ± 0.2[d]
14	6.46 ± 0.04	−1.8 ± 0.3	6.85 ± 0.07	−1.5 ± 0.3	6.06 ± 0.12	−1.0 ± 0.1	6.70 ± 0.06	−1.3 ± 0.2	6.06 ± 0.12	−1.1 ± 0.2
15	8.23 ± 0.11	−0.87 ± 0.12	9.74 ± 0.09	−0.97 ± 0.11	6.84 ± 0.08	−0.85 ± 0.05	9.35 ± 0.09	−0.83 ± 0.09	6.63 ± 0.03	−1.1 ± 0.1
16	7.86 ± 0.04	−1.8 ± 0.2[d]	8.52 ± 0.06	−1.9 ± 0.3	6.83 ± 0.03	−1.8 ± 0.02[d]	8.02 ± 0.23	−1.4 ± 0.1	6.41 ± 0.08	−1.3 ± 0.2
17	7.82 ± 0.04	−2.1 ± 0.1[d]	8.35 ± 0.04	−2.3 ± 0.2[d]	7.07 ± 0.06	−1.4 ± 0.1	7.73 ± 0.09	−1.5 ± 0.1[d]	7.16 ± 0.05	−1.5 ± 0.1[d]
18	8.00 ± 0.10	−1.9 ± 0.2[d]	8.87 ± 0.06	−1.3 ± 0.2	7.17 ± 0.01	−1.1 ± 0.03	8.40 ± 0.20	−1.3 ± 0.1	6.85 ± 0.01	−1.5 ± 0.1
20	8.54 ± 0.17	−1.4 ± 0.2	9.28 ± 0.09	−1.3 ± 0.1	7.09 ± 0.03	−0.99 ± 0.12	8.67 ± 0.18	−1.0 ± 0.1	6.87 ± 0.14	−0.99 ± 0.16
21	-		9.23 ± 0.10[c]	−0.82 ± 0.10	-		-		-	
22	-		9.03 ± 0.08	−1.4 ± 0.1	-		-		-	
23	8.28 ± 0.17	−1.3 ± 0.1	9.10 ± 0.04	−0.99 ± 0.19	6.81 ± 0.05	−1.3 ± 0.1[d]	8.35 ± 0.19	−0.98 ± 0.07	6.78 ± 0.24	−0.98 ± 0.15
26	-		9.57 ± 0.07	−1.9 ± 0.3	-		-		-	
27	-		8.85 ± 0.07	−1.5 ± 0.2	-		-		-	
28	8.64 ± 0.03	−1.6 ± 0.1[d]	9.20 ± 0.03	−1.3 ± 0.1	7.12 ± 0.02	−1.6 ± 0.2	8.54 ± 0.16	−1.1 ± 0.1	6.39 ± 0.02	−1.1 ± 0.4
29	8.79[e]	−1.2[e]	9.71[e]	−1.4[e]	7.77[e]	−1.2[e]	-		-	
30	8.64 ± 0.09	−1.6 ± 0.3	9.59 ± 0.03	−1.7 ± 0.2	7.66 ± 0.06	−1.2 ± 0.2	8.59 ± 0.04	−1.5 ± 0.3	7.51 ± 0.21	−0.70 ± 0.09

[a]Presented are mean values ± SEM from two (**23**, M_5R) or at least three independent experiments (performed in triplicate). K_d values (reported previously[42])/applied concentrations of [^{3}H]NMS: M_1, 0.12/0.2 nM; M_2, 0.090/0.2 nM; M_3, 0.089/ 0.2 nM; M_4, 0.035/0.1 nM; M_5, 0.24/0.3 nM. [b]Curve slope of the four-parameter logistic fit. [c]Data

were previously reported as pIC_{50} values by Keller *et al.* and were reanalyzed to give pK_i values.[42] [d]Slope different from unity ($P < 0.05$). [e]She *et al*.[39]

M_2R antagonism. The fluorescently labeled dibenzodiazepinone derivatives **18**, **20**, **23** and **28** were investigated in an IP1 accumulation assay at 37 °C using live HEK-293 cells transiently transfected with the hM_2R and the hybrid G-protein $G\alpha_{qi5\text{-}HA}$[38,52]. Compounds **18**, **20**, **23** and **28** did not elicit IP1 accumulation when studied in agonist mode (Figure 3A). In antagonist mode, **18**, **20**, **23** and **28** as well as the reference antagonist atropine (**31**) fully inhibited IP1 accumulation elicited by carbachol (CCh) (0.3 μM, ≈ EC_{80}) (Figure 3B), demonstrating that the studied fluorescent ligands are M_2R antagonists. As previously reported for the dibenzodiazepinone-type MR antagonists **6** and **7** (structures *cf*. Figure 1B), the antagonistic potencies of **18**, **20**, **23** and **28** (Table 2) were considerably lower compared to binding data (pK_i values) obtained from radioligand competition binding studies (Table 1). Increasing the incubation times in the M_2R IP1 assay from 30 min to 180 min (preincubation of the cells with antagonist) and from 60 min to 90 min (continued incubation after addition of the agonist CCh), as well as lowering the temperature from 37 °C to 22 °C during preincubation, did not affect (**18**, **28**) or led to a moderate increase (**20**, **23**) in pIC_{50} values (Table 2). Possibly, the type of interaction between **18**, **20**, **23** or **28** and CCh is different from how the small antagonist **31** inhibits the CCh induced IP1 accumulation, which is supported by a much better correlation of the pIC_{50} (pK_b) and pK_i value in case of **31** (pIC_{50}: 8.09 (Table 2), corresponding pK_b: 8.66, pK_i: 9.04 (Table 6)). Therefore, pK_b estimates were not calculated for **18**, **20**, **23** and **28**.

The fluorescent ligands **18**, **20**, **23** and **28** were also investigated in an M_4R IP1 accumulation assay using intact HEK-293 cells transiently transfected with the hM_4R and the hybrid G-protein $G\alpha_{qi5\text{-}HA}$. For these studies, only the aforementioned "long incubation" conditions (M_2R) were applied.

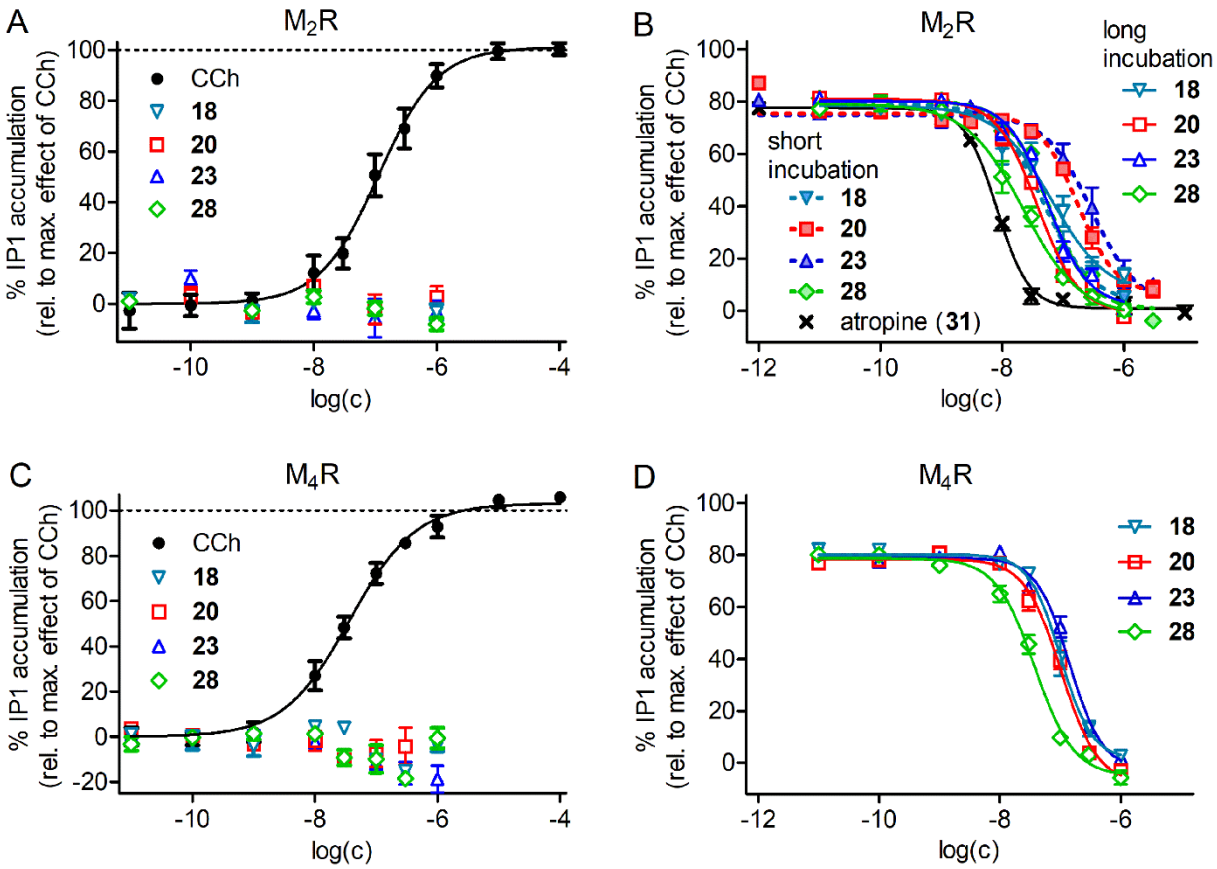

Figure 3. Investigation of M_2R and M_4R agonism and antagonism of compounds **18**, **20**, **23** and **28** in IP1 accumulation assays using HEK-hM_2-Gα_{qi5}-HA and HEK-hM_4-Gα_{qi5}-HA cells, respectively. (A) Effect of CCh, **18**, **20**, **23** and **28** on the M_2R mediated accumulation of IP1. **18**, **20**, **23** and **28** elicited no response. Data of CCh represent means ± SD from 14 independent experiments performed in duplicate. Data of **18**, **20**, **23** and **28** represent means ± SEM from three (**20**, **23**) or four (**18**, **28**) independent experiments performed in duplicate. pEC_{50} of CCh: 6.95 ± 0.12 (mean ± SD, n = 14). (B) Inhibition of the CCh (0.3 µM) induced IP1 accumulation (M_2R) by **18**, **20**, **23**, **28** and atropine (pIC_{50} values see Table 2). Cells were either preincubated with the antagonist at rt for 30 min followed by addition of CCh and continued incubation for 60 min (*short incubation*) or were preincubated with the antagonist at 22 °C for 180 min followed by addition of CCh and continued incubation at 37 °C for 90 min (*long incubation*). Data represent means ± SEM (number of individual experiments see Table 2). (C) Effect of CCh, **18**, **20**, **23** and **28** on the M_4R mediated accumulation of IP1. **18**, **20**, **23** and **28** elicited no response. Data represent means ± SEM from four (**18**, **20**, **23**, **28**) or six (CCh) independent

experiments, each performed in duplicate. pEC_{50} of CCh: 7.42 ± 0.02 (mean ± SEM, n = 6). (D) Inhibition of the CCh (0.1 μM) induced IP1 accumulation (M_4R) by **18**, **20**, **23**, **28** (pIC_{50} values see Table 2). Cells were preincubated with the antagonist at 22 °C for 180 min followed by addition of CCh and continued incubation at 37 °C for 90 min. Data represent means ± SEM (number of individual experiments see Table 2).

As in case of the M_2R IP1 assay, compounds **18**, **20**, **23** and **28** did not elicit IP1 accumulation when studied in agonist mode (Figure 3C), but completely inhibited IP1 accumulation elicited by carbachol (0.1 μM, ≈ EC_{80}) when studied in antagonist mode (Figure 3D). The pIC_{50} values from the M_4R IP1 assay were marginally lower than the respective pIC_{50} values obtained from the M_2R IP1 assay (Table 2), reflecting lacking M_2R selectivity (towards M_4R) identified in radioligand competition binding studies (Table 1).

Table 2. Antagonistic activities of **18**, **20**, **23** and **28** obtained from M_2R and M_4R IP1 accumulation assays.

compd.	M_2R				M_4R	
	short incubation		long incubation		long incubation	
	pIC_{50}[a]	n[b]	pIC_{50}[a]	n[b]	pIC_{50}[c]	n[b]
18	7.31 ± 0.15	4	7.22 ± 0.12	9	7.04 ± 0.09	8
20	6.65 ± 0.09	6	7.41 ± 0.05	7	6.99 ± 0.07	6
23	6.45 ± 0.14	6	7.24 ± 0.05	7	6.86 ± 0.03	6
28	7.62 ± 0.19	4	7.76 ± 0.12	8	7.43 ± 0.04	10
31 (atropine)	8.09 ± 0.03	5	n.d.	-	n.d.	-

[a]Inhibition of the CCh (0.3 μM, ≈ EC_{80}) induced IP1 accumulation in HEK-hM_2-G$\alpha_{qi5\text{-}HA}$ cells. Cells were preincubated with the antagonist at rt for 30 min followed by addition of CCh and continued incubation for 60 min (short incubation), or were preincubated with the antagonist at 22 °C for 180 min followed by addition of CCh and continued incubation at 37 °C for 90 min (long incubation). Inhibition curves are shown in Figure 3. Data represent mean values ± SEM from n independent experiments. [b]Number of individual experiments (each performed in duplicate). [c]Inhibition of the CCh (0.1 μM, ≈ EC_{80}) induced IP1 accumulation in HEK-hM_4-G$\alpha_{qi5\text{-}HA}$ cells. Cells were preincubated with the antagonist at 22 °C for 180 min followed by addition of CCh and continued incubation at 37 °C for 90 min. Inhibition curves are shown in Figure 3. Data represent mean values ± SEM from n independent experiments.
n.d.: not determined

Fluorescence properties. The fluorescence quantum yields were determined (reference: cresyl violet perchlorate) for the fluorescent ligands **16-18**, **20**, **22**, **23** and **28** in PBS (pH 7.4) and in PBS supplemented with 1% bovine serum albumin (BSA) to estimate the influence of proteins on the quantum yield (Table 3). The selected set of compounds covered all types of fluorophores used in this work. All investigated fluorescent ligands showed a higher quantum yield in PBS supplemented with 1% BSA compared to PBS alone (Table 3). This phenomenon was previously observed for fluorescently labeled NPY Y_1 and Y_4 receptor ligands, too,[12,14] and can be explained by interactions (hydrophobic, electrostatic) of the fluorophores with the protein, resulting in a changed chemical environment and reduced molecular motion (increased rigidity) of the fluorophore.

Table 3. Fluorescence properties of the MR ligands **16-18**, **20**, **22**, **23** and **28** in PBS and PBS containing 1% BSA: excitation/emission maxima and fluorescent quantum yields Φ (reference: cresyl violet perchlorate).

compd.	type/net charge of cyanine dye (*cf.* Figure 2)	PBS		PBS + 1% BSA	
		$\lambda_{ex}/\lambda_{em}$ [nm]	Φ (%)	$\lambda_{ex}/\lambda_{em}$ [nm]	Φ (%)
16	pyridinium/+1	460/713	8.9	484/643	23.8
17	indolinium/+1	645/663	19.1	655/675	42.1
18	indolinium/0	648/665	20.9	660/678	30.1
20	indolinium/−1	653/669	17.7	656/672	29.0
22	indolinium/0	645/666	24.4	663/676	51.1
23	indolinium/−1	651/669	21.6	658/673	36.8
28	indolinium/−1	650/668	-[a]	658/673	43.4

[a]Due to the strong adsorption of **28** to the cuvette when dissolved in PBS without BSA, the determination of Φ failed.

Excitation and corrected emission spectra of **16-18**, **20**, **22**, **23** and **28** in PBS containing 1% BSA (Figure S2, Supporting Information) revealed that the pyridinium-type fluorescent ligand **16** can be excited with an argon laser and the indolinium-type cyanine dye labeled compounds (**17**, **18**, **20**, **22**, **23** and **28**) are suited for an excitation with a red diode laser (635 nm).

Flow cytometric binding studies. The fluorescent ligands **18**, **20**, **23**, **28** and **30** were applied in flow cytometric saturation binding studies using intact CHO-hM_2R cells. The obtained pK_d values of 8.59, 9.05, 8.35, 8.51 and 9.19, respectively (Table 4), were in good agreement with the binding data from competition binding studies with [^{3}H]NMS (*cf.* Table 1). At concentrations corresponding to the K_d value, unspecific binding was around 10% (**18**, **20**, **23**, **30**) or below 5% (**28**) of totally bound fluorescent ligand (Figure 4). The saturation binding experiments revealed that **18**, **20**, **23**, **28** and **30** bind to the orthosteric binding site of the hM_2R, because the orthosteric antagonist atropine (**31**) (for structure see Figure S4, Supporting Information), used to determine unspecific binding, was capable of completely preventing one-site (monophasic) specific M_2R binding of these fluorescent ligands. Saturation binding experiments with **20** were also performed at CHO-hM_1R and CHO-hM_4R cells, yielding pK_d values of 8.19 and 8.02, respectively (Table 4; Figure S5, Supporting Information), which were again in good accordance with binding data from radioligand competition binding studies (*cf.* Table 1).

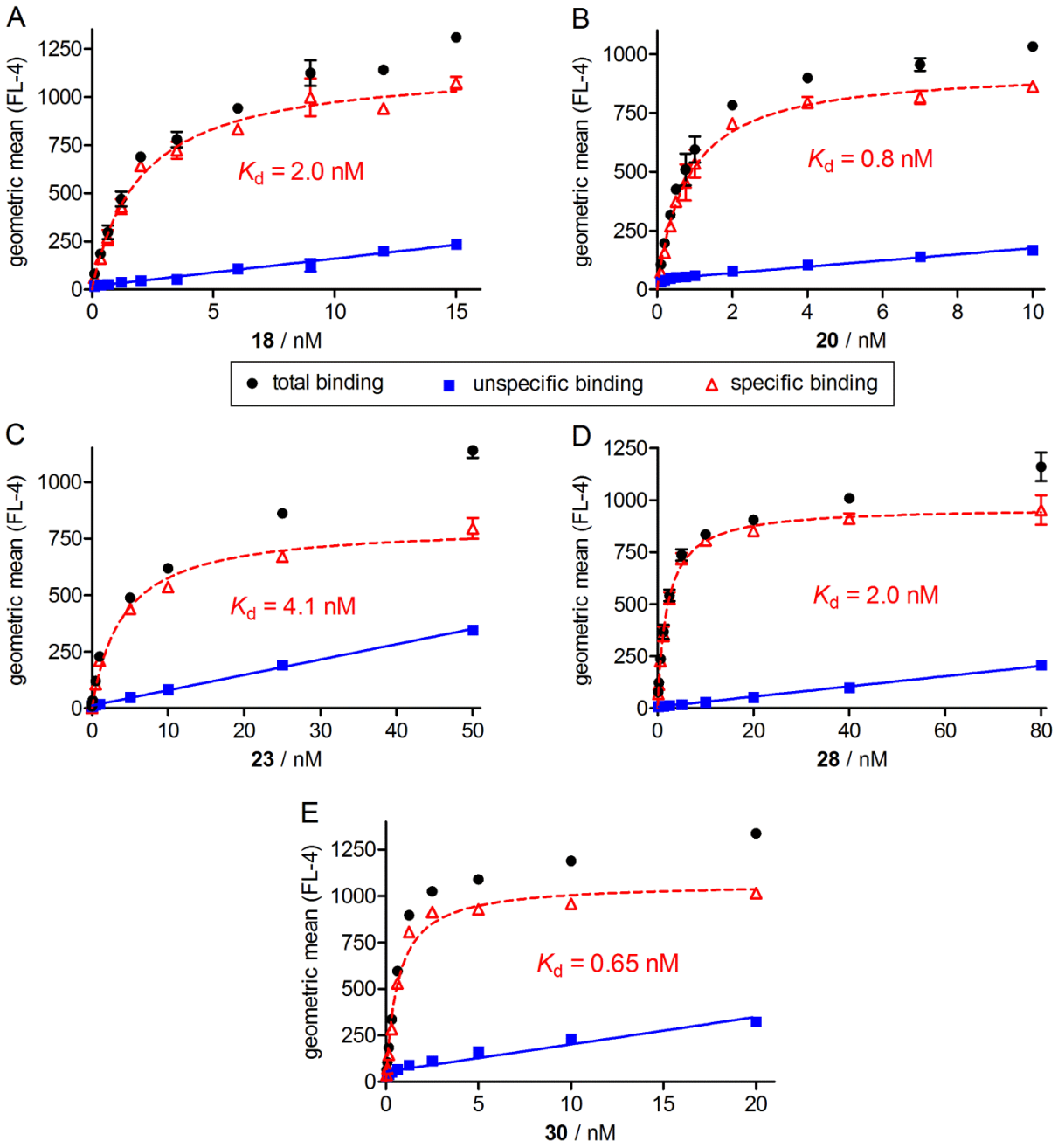

Figure 4. Representative saturation isotherms (specific binding, dashed line) obtained from flow cytometric saturation binding experiments performed with **18** (A), **20** (B), **23** (C), **28** (D) and **30** (E) at intact CHO-hM_2R cells. Unspecific binding was determined in the presence of atropine (**31**, for structure see Figure S4, Supporting Information) (500-fold excess to **18**, **20**, **23**, **28** or **30**). Cells were incubated with the fluorescent ligands at 22 ˚C in the dark for 2 h (experiments performed in duplicate). Measurements were performed with a FACSCalibur flow cytometer (Becton Dickinson). In the case of total and unspecific binding, data represent mean

values ± SEM. In the case of specific binding, data represent calculated values ± propagated error.

Table 4. M_1R binding data of **20**, **23** and **28**, M_2R binding data of **18**, **20**, **23**, **28** and **30**, and M_4R binding data of **20** determined by saturation binding.

fluorescent ligand	pK_d[a] (flow cytometry)		
	hM_1R	hM_2R	hM_4R
18	-	8.59 ± 0.09	-
20	8.19 ± 0.02	9.05 ± 0.04	8.02 ± 0.03
23	-	8.35 ± 0.06	-
28	-	8.51 ± 0.08	-
30	-	9.19 ± 0.02	-
	pK_d[a] (high-content imaging)		
	hM_1R	hM_2R	-
18	-	8.06 ± 0.04	
20	-	8.33 ± 0.03	
23	7.58 ± 0.04	7.94 ± 0.02	
28	8.00 ± 0.05	8.25 ± 0.04	

[a]Determined by saturation binding at intact CHO-hM_xR cells (x = 1,2,4) at 22 °C using a FACSCalibur flow cytometer or an IX Ultra Confocal Plate Reader (high-content imaging); mean values ± SEM (pK_d) from at least two independent experiments performed in duplicate (flow cytometry) or triplicate (high-content imaging).

The association and dissociation kinetics of **20**, **23** and **28** were determined by flow cytometry at intact CHO-hM_2R cells at 22 °C using ligand concentrations which corresponded approximately to the K_d values of **20**, **23** and **28** determined by flow cytometry at CHO-hM_2R cells (*cf.* Table 4). The association of **20**, **23** and **28** to the M_2R appeared to be monophasic (Figure 5, k_{obs} and k_{on} values summarized in Table 5). For M_2R dissociation studies with **20**, **23** and **28**, cells were preincubated with the fluorescent ligand for 180, 120 and 110 min, respectively, applying ligand concentrations corresponding approximately to three times the K_d. The dissociations of **20**, **23** and **28** were followed over 9 h. Data analysis by a three-parameter

equation described an incomplete monophasic decline (k_{off} values given in Table 5). The dissociation plateaus were different from zero (one-tailed t-test, $P < 0.05$ (**20**, **23**) or < 0.02 (**28**)), indicating a minor component of long lasting M_2R binding of the studied fluorescent ligands (observed plateau values: 23%, 5% and 22%, respectively; Figure 5). Such a phenomenon can be explained by conformational adjustments of the receptor upon ligand binding[53] or by an enhanced rebinding mediated by a simultaneous interaction with more than one binding site.[54] The kinetically derived dissociation constants K_d(kin) of **20**, **23** and **28** were in good agreement with the K_d values obtained from flow cytometric saturation binding studies (Table 5).

Compound **23**, showing the fastest dissociation of the studied ligands (**20**, **23**, **28**) was chosen to perform dissociation experiments in the presence of the allosteric M_2R modulators W84 (**32**),[55-57] LY2119620 (**33**)[58,59] or alcuronium (**34**)[60,61] (Structures see Figure S4, Supporting Information). The allosteric ligands, used at a high concentration of 100 μM, did not reduce the observed dissociation rate of **23** from the M_2R as previously observed for the structurally related radioligands [^{3}H]**6** and [^{3}H]**7**.[38] These results are consistent with competitive interactions and an overlapping binding site between **23** and the allosteric modulators **32-34**. They suggest a dualsteric binding mode of **23** to the orthosteric and allosteric pocket at the M_2R, and by implication a similar mode of action for the structurally related fluorescent M_2R ligands **10**, **12**, **14**, **16-18**, **20**, **22**, **27**, **28** and **30**.

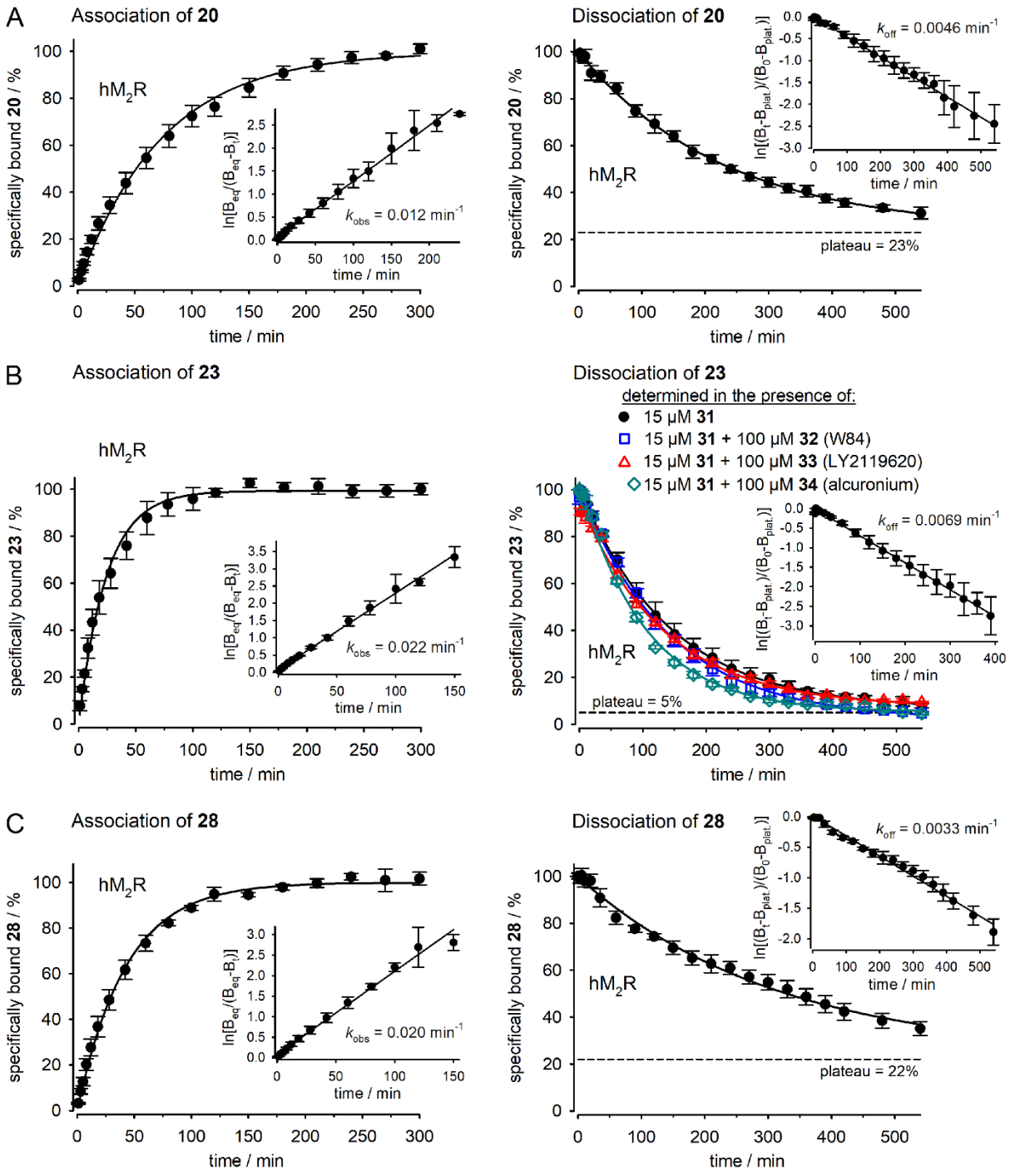

Figure 5. Association and dissociation kinetics of **20** (panel A), **23** (panel B) and **28** (panel C) determined by flow cytometry at intact CHO-hM_2R cells at 22 °C. The dissociation was determined in the presence of an excess of atropine (**31**). (A, left) Association of **20** (1 nM) to the M_2R; inset: $\ln[B_{eq}/(B_{eq}-B_t)]$ versus time. (A, right) Dissociation of **20** (preincubation: 3 nM, 180 min) from the M_2R. (B, left) Association of **23** (5 nM) to the M_2R; inset: $\ln[B_{eq}/(B_{eq}-B_t)]$

versus time. (B, right) Dissociation of **23** (preincubation: 15 nM, 120 min) from the M_2R. Addition of the allosteric M_2R modulators **32**, **33** or **34** at a high concentration (100 μM) did not slow down the dissociation of **23** indicating a competitive mechanism between **23** and the allosteric M_2R ligands. (C, left) Association of **28** (3.5 nM) to the M_2R; inset: $\ln[B_{eq}/(B_{eq}-B_t)]$ versus time. (C, right) Dissociation of **28** (preincubation: 10 nM, 110 min) from the M_2R. Data in A-C represent the mean ± SEM from three or four independent experiments (performed in duplicate). Dissociation data were analyzed by a three-parameter equation describing an incomplete monophasic decline because the curve plateau mean values (23%, 5% and 22%, respectively) from individual experiments (analyzed by a three-parameter equation) were different from zero ($P < 0.05$, < 0.05 and < 0.02, respectively). The association and dissociation rate constants derived from non-linear curve fitting are summarized in Table 5.

Table 5. Parameters characterizing the association of **20**, **23** and **28** to, and their dissociation from the hM_2R, determined at CHO-hM_2R cells at 22 ± 1 °C.

compd.	K_d(sat) [nM][a]	K_d(kin) [nM][b]	k_{obs} [min^{-1}][c]	k_{on} [$min^{-1} \cdot nM^{-1}$][d]	k_{off} [min^{-1}][e]
20	0.91	0.48 ± 0.22	0.014 ± 0.002	0.0095 ± 0.0028	0.0045 ± 0.0007
23	4.6	1.9 ± 0.6	0.026 ± 0.001	0.0037 ± 0.0005	0.0069 ± 0.0011
28	3.2	1.4 ± 0.5	0.024 ± 0.003	0.0049 ± 0.0011	0.0031 ± 0.0004

[a]Dissociation constant (given for comparison with K_d(kin)) determined by flow cytometric saturation binding at CHO-hM_2R cells (data taken from Table 4). [b]Kinetically derived dissociation constant (± propagated error) calculated from k_{on} and k_{off}. [c]Observed association rate constant obtained from two-parameter non-linear fits (exponential rise to a maximum); mean values ± SEM from three (**23**, **28**) or four (**20**) independent experiments performed in duplicate. [d]Association rate constant ± propagated error, calculated from k_{obs}, k_{off} and the applied radioligand concentration (*cf.* Figure 5 and experimental section). [e]Dissociation rate constant obtained from three-parameter non-linear fits (incomplete monophasic exponential decline); mean ± SEM from three (**20**, **28**) or four (**23**) independent experiments performed in duplicate.

Confocal microscopy. Binding studies with compounds **20**, **23** and **28** at live CHO-hM_2R cells, using confocal microscopy, revealed a marked difference between total and unspecific binding in all cases (Figure 6). Over the whole incubation period (45 min), the major fraction of detected

fluorescence appeared to be associated with the plasma membrane, and a substantial increase in intracellular fluorescence over time was not observed.

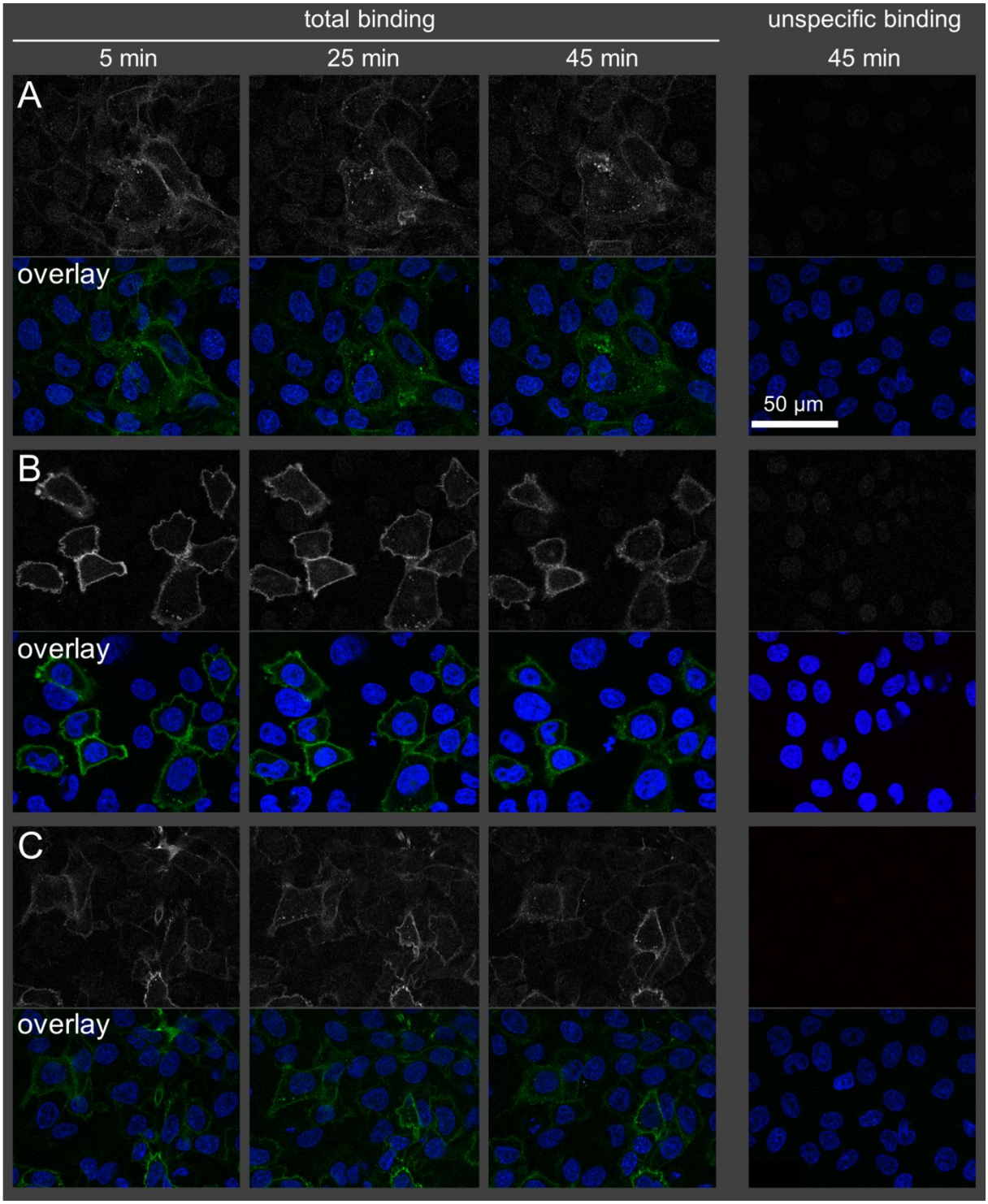

Figure 6. Binding of the fluorescent ligands **20** (A), **23** (B) and **28** (C) (each 30 nM) to live CHO-hM_2R cells at 30 °C, visualized by confocal microscopy (excitation: 633 nm, emission:

638-759 nm) after 5, 25 and 45 min. Unspecific binding was determined in the presence of atropine (**31**, 10 μM). Upper panels show ligand fluorescence alone (greyscale) and overlay panels merge ligand fluorescence (green) and nuclei (blue). Images (representative of at least three experiments) were acquired with a Zeiss LSM 710 confocal microscope.

High-content imaging. The fluorescent ligands **18**, **20**, **23** and **28** were also applied in high-content imaging binding assays, allowing a higher sample throughput compared to flow cytometers. In order to reduce background fluorescence, a wash step was performed immediately before measurement (exemplified for **23** in Figure S8, Supporting Information) Saturation binding experiments with **18**, **20**, **23** and **28** at live CHO-hM_2R cells revealed pK_d values (8.06, 8.33, 7.94 and 8.25, respectively), which were slightly lower compared to pK_d values obtained by flow cytometric saturation binding studies (Table 4, Figure 7). These deviations might be attributed to the different techniques used, requiring different types of fluorescence analysis (flow cytometry: analysis of single, suspended cells passing a laser beam; high-content imaging: acquisition of fluorescence images of adherent cells, fluorescence quantification by granularity analysis). Moreover, in case of high-content imaging, high unspecific binding at higher fluorescent ligand concentrations (*cf*. Figure S8, Supporting Information) might affect the free concentration of fluorescent ligand, resulting in lower apparent pK_d values.

In addition to M_2R binding studies, saturation binding experiments with **23** and **28** were performed at CHO-hM_1R cells (Figure S6, Supporting Information) yielding pK_d values of 7.58 and 8.00, respectively (Table 4). Binding experiments with reference compound **25** at CHO-hM_2R cells revealed that the fluorescent dye itself was not capable of staining the cells (Figure S9, Supporting Information).

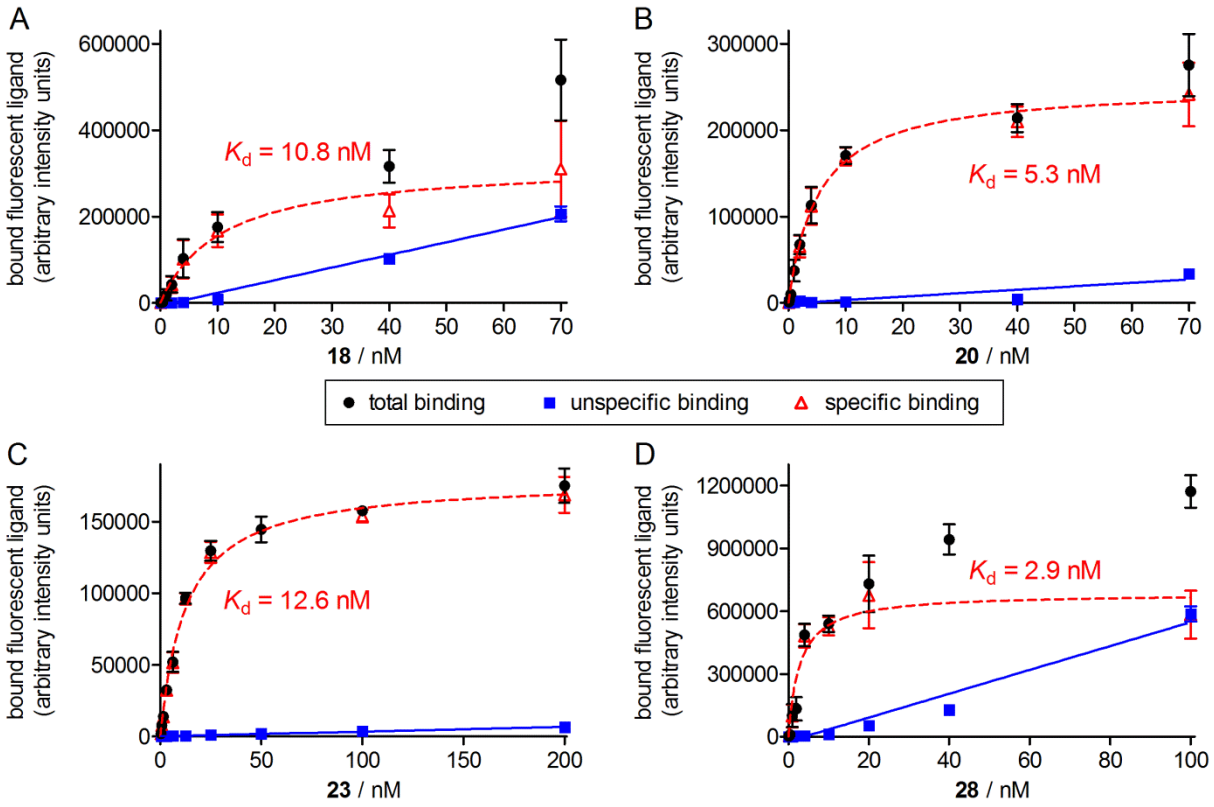

Figure 7. Representative saturation isotherms (specific binding, dashed line) obtained from high-content imaging saturation binding experiments performed with **18** (A), **20** (B), **23** (C) and **28** (D) at intact CHO-hM_2R cells. Unspecific binding was determined in the presence of atropine (500-fold excess to **18**, **20**, **23** or **28**). Cells were incubated with the fluorescent ligands at 22 °C in the dark for 1 h followed by a wash step and immediate measurement with an IX Ultra Confocal Plate Reader (Molecular Devices). Experiments were performed in triplicate. In the case of total and unspecific binding, data represent mean values ± SEM. In the case of specific binding, data represent calculated values ± propagated error.

In order to further support the hypothesis of dualsteric binding of the fluorescent ligands to the M_2R (concluded, e.g. from dissociation experiments with **23** in the presence of various allosteric M_2R modulators; see Figure 5B), saturation binding experiments were performed with **20**, **23** and **28** in the presence of the negative allosteric M_2R modulator **32** (structure see Figure S4,

Supporting Information),[55-57] applied at increasing concentrations (Schild-like analysis, Figure 8). This kind of experiment is equivalent to the Schild analysis used to investigate the inhibiting effect of a receptor antagonist on the response elicited by an agonist,[62-64] and was applied, for instance, to prove the dualsteric binding mode of [^{3}H]**6** and [^{3}H]**7** at the hM_2R[38,39] as well as of a fluorescent pirenzepine derivative at the M_1R.[31] In the presence of **32**, the saturation isotherms of both monomeric ligands (**20**, **23**) and of the dimeric ligand **28** were rightward shifted resulting in linear 'Schild' regressions with a slope not different from unity (Figure 8; Table S1, Supporting Information). These results were further indication of a competitive mechanism between the allosteric M_2R ligand **32** and the fluorescent dibenzodiazepinone-type ligands **20**, **23** and **28**.

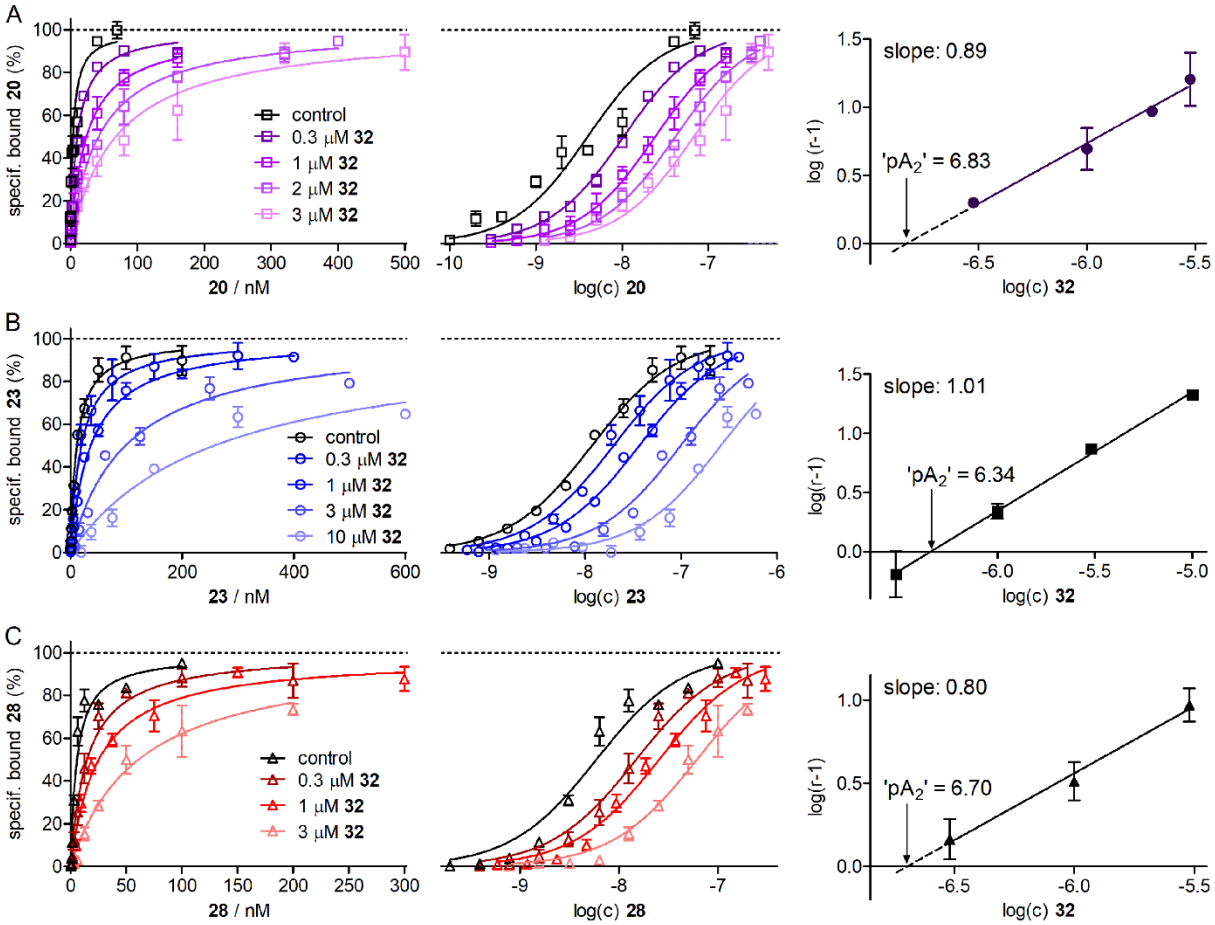

Figure 8. Saturation binding of **20** (A), **23** (B) and **28** (C) at the hM_2R in the presence of the allosteric M_2R modulator **32** (for structure see Figure S4, Supporting Information) determined at intact CHO-hM_2R cells using high-content imaging. Presented are saturation isotherms of specific fluorescent ligand binding (left, linear scale; middle, semi-logarithmic scale) and 'Schild' regressions (right) resulting from the rightward shifts (ΔpK_d) of the saturation isotherms (log(r−1) plotted vs. log(concentration allosteric modulator), where $r = 10^{\Delta pKd}$). Increasing concentrations of **32** resulted in a rightward shift of the saturation isotherms of the fluorescently labeled dibenzodiazepinone derivatives **20**, **23** and **28**. In all cases, the slope of the linear "Schild" regression was close to unity (for statistical evaluation see Table S1, Supporting Information), indicating a competitive interaction between the fluorescent ligands and the allosteric modulator **32**. Data represent mean values ± SEM from three independent experiments (performed in triplicate). Note: In case of the logistic (sigmoidal) fits (middle), initial four parameter fitting to allow variation in the Hill factor, did not result in slopes

significantly different from unity ($P > 0.05$) except for '**20** + 2 μM **32**' (slope = 0.94 ± 0.01, $P < 0.02$) and '**23** + 0.3 μM **32**' (slope = 1.23 ± 0.04, $P < 0.05$). As these slopes were still close to unity, the data were also analyzed using a fixed slope of 1, which did not affect the respective pK_d values (deviations < 0.2%).

The 'pA_2' values of **32** derived from the 'Schild' regressions were in good agreement with a reported 'pA_2' of **32**[38] and with the pK_i values of **32** from equilibrium competition binding studies with **20**, **23** and **28** (described below; Table S1, Supporting Information). With regard to the fact that **20**, **23** and **28** address the orthosteric binding site of the M_2R (concluded from experimental data presented in Figures 4 and 7) the results of the Schild-like analyses suggested, as already reported, e.g. for the dibenzodiazepinone-type MR ligands **6** and **7**,[38,39] a dualsteric binding mode of **20**, **23** and **28** at the hM_2R.

Fluorescence-based competition binding studies. The fluorescent probes **18**, **20**, **23** and **28** were applied in competition binding studies at CHO-hM_2R cells to determine M_2R affinities of various reported MR ligands, including orthosteric antagonists (NMS, atropine (**31**)), orthosteric agonists (xanomeline (**35**), oxotremorine (**36**)), allosteric modulators (W84 (**32**),[55] LY2119620 (**33**)[58,59]), and dualsteric ligands (**6**, UR-AP060 (**37**),[38] AF-DX 384 (**38**)[65,66]) (for structures see Figure S4, Supporting Information, and Figure 1B). In high-content imaging binding assays, NMS, compounds **6**, **31-33** and **35-37** fully competed for specific hM_2R binding of **20**, **23** or **28**, indicating a competitive mechanism between the reported MR ligands and **20**, **23** and **28** (*cf*. Figure S7B-S7D, Supporting Information). As the allosteric M_2R ligands **32** and **33** were capable of complete displacement of **20**, **23** and **28** at the hM_2R, these results support the hypothesis of a dualsteric binding mode of **20**, **23** and **28** at the hM_2R, and are consistent with the results from the Schild analysis (Figure 8). Flow cytometric competition binding experiments with **20** and the reported MR ligands **6**, **31-33**, **35** and **38** also resulted throughout

in complete displacement of **20** (Figure S7E and S7F, Supporting Information). The reference compound pK_i values (NMS, **6**, **31-33**, **35-38**) against different fluorescent tracers (**18**, **20**, **23** or **28**) were also compared with the pK_i values obtained from orthosteric radioligand ([^{3}H]NMS) competition binding experiments. Here, the closest correlation between fluorescent and radioligand data was observed when using fluorescent ligand **23** (Table 6). One explanation may be the nearly fully reversible M_2R binding of **23**, compared to the persistence of a long lasting pseudo-irreversible component identified in **20** and **28** dissociation experiments (Figure 5).

To discriminate between a competitive and an allosteric interaction of the allosteric M_2R modulator **32** and the dibenzodiazepinone-type fluorescent MR ligands, the effect of **32** on hM_2R equilibrium binding of **20**, applying a high M_2R occupancy by **20** (c = 20 nM, K_d = 0.91 nM, fractional receptor occupancy: 0.96), was determined. In case of a negative allosteric mechanism between **32** and **20**, this type of experiment would result in an elevation of the lower curve plateau (four-parameter logistic fit), and the pIC_{50} value of **32** would be unaffected compared to the experiment using a concentration of **20** close to its K_d value (such a non-competitive behavior was previously demonstrated, e.g., for [^{3}H]NMS and **32**[38]). However, as shown in Figure S7F (Supporting Information), the lower curve plateau did not increase and the pIC_{50} of **32** was rightward shifted by approx. one order of magnitude, being consistent with a competitive mechanism between **20** and **32**.

Table 6. M_2R binding data (pK_i or pIC_{50}) of various orthosteric (NMS, **31**, **35**, **36**), allosteric (**32**, **33**) and dualsteric (**6**, **37**, **38**) MR ligands determined by the use of the fluorescent ligands **18**, **20**, **23** or **28**, and with the orthosteric radioligand [^{3}H]NMS.

compd.	labeled ligand used for competition binding studies					
	20	**18**	**20**	**23**	**28**	[^{3}H]NMS
	$pK_i \pm$ SEM[a] *slope ± SEM*[b] (flow cytometry)	$pK_i \pm$ SEM[c] *slope ± SEM*[b] (high-content imaging)				pK_i* or pIC_{50}** (radiochemical)
NMS	-	8.95 ± 0.13 *−1.7 ± 0.2*[d]	8.93 ± 0.14 *−1.6 ± 0.5*	9.86 ± 0.17 *−1.1 ± 0.2*	9.23 ± 0.08 *−0.83 ± 0.01*[d]	10.01 ± 0.08*[e]
6	8.70 ± 0.05 *−0.96 ± 0.33*	-	-	9.00 ± 0.28 *−1.0 ± 0.04*	8.39 ± 0.17 *−1.2 ± 0.1*	9.12*[f]
31 (atropine)	8.60 ± 0.21 *−0.78 ± 0.16*	7.73 ± 0.07 *−0.89 ± 0.37*	8.31 ± 0.08 *−1.2 ± 0.2*	8.50 ± 0.11 *−0.79 ± 0.05*	8.15 ± 0.07 *−1.1± 0.1*	9.04 ± 0.08*[e]
32 (W84)	6.39 ± 0.09 *−0.78 ± 0.05*	-	5.85 ± 0.08 *−0.88 ± 0.11*	6.19 ± 0.16 *−1.1 ± 0.3*	6.07 ± 0.08 *−1.2 ± 0.3*	6.32**[f]
33 (LY2119620)	5.19 ± 0.07 *−1.5 ± 0.1*	-	5.45 ± 0.21 *−1.9 ± 0.3*	5.04 ± 0.06 *−1.8 ± 0.1*[d]	5.03 ± 0.20 *−1.0 ± 0.2*	< 4.5**[f]
35 (xanomeline)	6.67 ± 0.02 *−1.1 ± 0.2*	6.14 ± 0.01 *−1.4 ± 0.3*	6.42 ± 0.03 *−1.6 ± 0.4*	6.49 ± 0.15 *−1.1 ± 0.1*	6.56 ± 0.14 *−1.0 ± 0.2*	6.70 ± 0.16*[e]
36 (oxotremorine)	-	-	6.07 ± 0.19 *−1.1 ± 0.5*	5.99 ± 0.03 *−0.86 ± 0.24*	5.75 ± 0.04 *−1.0 ± 0.3*	7.04 ± 0.12*[e]
37 (UR-AP060)	-	-	-	9.45 ± 0.13 *−1.1 ± 0.04*	9.28 ± 0.18 *−1.5 ± 0.4*	9.39*[f]
38 (AF-DX 384)	8.31 ± 0.18 *−0.75 ± 0.12*	-	-	-	-	8.71 ± 0.04*[e]

[a]Determined by flow cytometric competition binding experiments with **20** (1 nM) at live CHO-hM_2R cells; mean values ± SEM from at least two independent experiments (performed in duplicate). [b]Curve slope of the four-parameter logistic fit. [c]Determined by high-content imaging competition binding with **18** (10 nM), **20** (10 nM), **23** (10 nM) or **28** (10 nM) at intact CHO-hM_2R cells; mean values ± SEM from at least two independent experiments (performed in duplicate). [d]Slope different from unity ($P < 0.05$). [e]Determined by competition binding studies with [^{3}H]NMS (c = 0.2 nM) at live CHO-hM_2R cells; mean values ± SEM from at least two independent experiments (performed in triplicate). [f]Pegoli *et al*,[38] pIC_{50} values were not converted to pK_i values as **32** and **33** inhibit [^{3}H]NMS binding in a non-competitive manner.

Molecular dynamics (MD) simulations. To model the interactions between the fluorescent dibenzodiazepinone derivatives and the M_2R, MD simulations (5 μs) of the human M_2R bound to the fluorescent ligands **23** or **28** were performed by analogy with a MD simulation described for **6**.[38] It should be noted that such short scale MD simulations, starting from a docking pose and requiring numerous simplifications, can only give a vague idea of the binding mode, but

are by far incapable of describing the whole ligand binding process. According to the simulation data, both ligands exhibited comparable orthosteric receptor interactions, which were persistent over the whole simulation timeframe (Figure 9A and 9B, Figure S10B, Supporting Information). The allosteric vestibule ('common' allosteric site) of the hM_2R was primarily occupied by the linker moieties in **23** and **28** (Figure 9A and 9B), but not by the fluorophores. This supports the competitive pharmacological interaction between the fluorescent ligands and the allosteric modulator **32** at the hM_2R (*cf.* Figures 5B and 8, and Figure S7F, Supporting Information). The monomeric ligand **23** showed no persistent hydrogen bonds except for those in the orthosteric binding site, but a cation-π interaction with $W422^{7.35}$, a key residue involved in binding of allosteric MR modulators,[67] was evident as "allosteric contact" (Figure 9A, Figure S10B, Supporting Information). In case of the homodimeric fluorescent ligand **28**, hydrogen bonds to $T84^{2.65}$, $D173^{ECL2}$ and $E175^{ECL2}$, located in the allosteric vestibule and in ECL2, respectively, were identified as allosteric interactions (Figure 9B, Figure S10B, Supporting Information). Whereas the fluorophore and a part of the linker of **23** showed high flexibility over the whole time period of the simulation (Figure 9C), the non-orthosterically bound part of the dimeric ligand **28** proved to be considerably less flexible (Figure 9D). This was also evident from an RMSD analysis of **23** and **28** (Figure S11, Supporting Information), although one has to keep in mind that the RMSD analysis considers the entire ligand structure. As reported previously for a MD simulation of the hM_2R bound to compound **6**, the highly conserved $D103^{3.32}$, which typically interacts with MR agonists,[68] formed a cluster with $S76^{2.57}$, $W99^{3.28}$, $Y426^{7.39}$ and $Y430^{7.43}$ (Figure S10A, Supporting Information) instead of interacting with the antagonists **23** and **28**. This was also reported for crystal structures of the M_1R and M_4R in complex with an antagonist.[69]

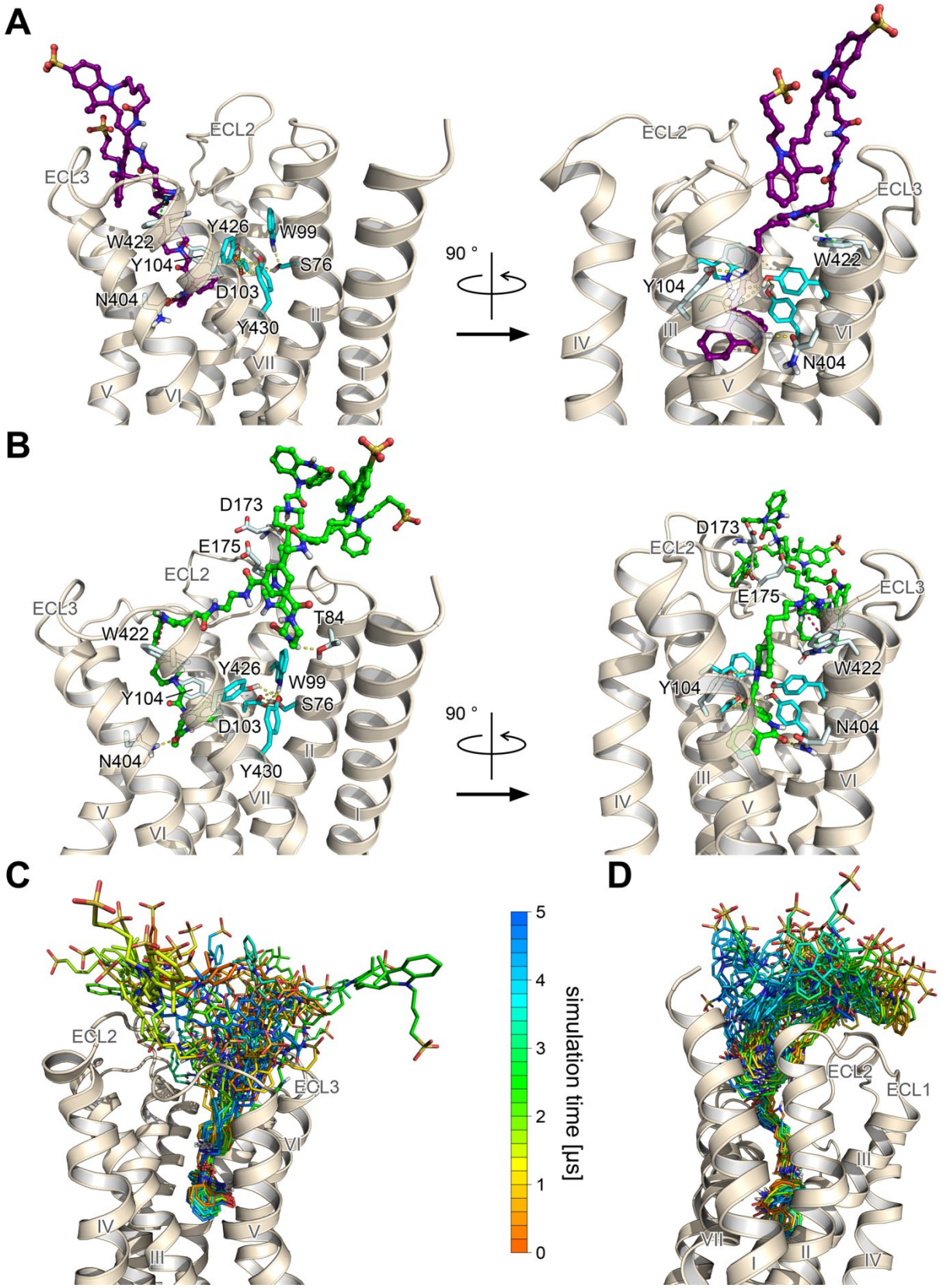

Figure 9. Molecular dynamics simulations (5 µs) of the human M_2R (inactive state, PDB code 3UON[70]) bound to the fluorescent dibenzodiazepinone derivatives **23** (A, C) or **28** (B, D). (A) Cluster 0 binding pose of **23** (shown in purple). (B) Cluster 0 binding pose of **28** (shown in

green). In A and B, carbon atoms of amino acids constituting the D103$^{3.32}$/S76$^{2.57}$/W99$^{3.28}$/Y426$^{7.39}$/Y430$^{7.43}$ cluster are highlighted in cyan. H-bonds between ligand and receptor (yellow dashed lines) were identified for Y104$^{3.33}$ (o.) and N404$^{6.52}$ (o.) (A), as well as for T84$^{2.65}$ (a.), Y104$^{3.33}$ (o.), D173^{ECL2} (a.), E175^{ECL2} (a.) and N404$^{6.25}$ (o.) (B). In A, π−π-stacking (a.) between ligand and receptor is highlighted as green dashed line, and in B, the cation−π-interaction (a.) between ligand and receptor is highlighted as pink dashed line. (C, D) Time course of the 5 µs MD simulations of the hM_2R bound to **23** (C) or **28** (D) showing superimposed snap shots collected every 200 ns. o. = orthosteric, a. = allosteric.

Conclusion

The study presents a series of fluorescence-labeled dibenzodiazepinone-type, M_2R subtype-preferring MR antagonists, comprising compounds with high M_2R affinity (pK_i > 8.5). Saturation binding and dissociation experiments at the M_2R in the absence and in the presence of allosteric M_2R ligands suggested a dualsteric binding mode at the M_2R. The application of the presented type of fluorescent probes in flow cytometric and high-content imaging binding assays as well to confocal microscopy, revealed their suitability as molecular tools to study M_2R expression in cells and to determine M_2R binding affinities of (non-labeled) orthosteric and allosteric M_2R ligands. As the presented fluorescent M_2R ligands lack selectivity towards the M_1 and M_4 receptor, this compound class might be useful for the design and preparation of fluorescent probes with high M_1R, M_2R or M_4R affinity, using fluorophores with properties compatible with fluorescence based techniques such as (time-resolved-)FRET measurements, fluorescence correlation spectroscopy and fluorescence anisotropy based methods. On the other hand, the combination of fluorescence labeling with a recently reported approach to increase M_2R selectivity of dibenzodiazepinone-type MR ligands[71] might lead to M_2R selective fluorescent probes.

Experimental section

General experimental conditions. Standard chemicals and solvents were purchased from commercial suppliers and were used without further purification. Acetonitrile for HPLC (gradient grade) was obtained from Merck (Darmstadt, Germany) or Sigma-Aldrich (Taufkirchen, Germany). CCh, NMS, atropine (**31**), W84 (**32**) and Hoechst 33342 (H33342) were purchased from Sigma-Aldrich. Oxotremorine sesquifumarate (**36**) was from MP Biomedicals (Eschwege, Germany) and LY2119620 (**33**) was purchased from Absource Diagnostic (Munich, Germany). AF-DX 384 (**38**) was from Abcam (Cambridge, UK). The indolinium-type cyanine dye succinimidyl esters **11**, **13** and **19** were obtained from FEW Chemicals (Bitterfeld-Wolfen, Germany). [^{3}H]NMS (specific activity = 80 Ci/mmol) was purchased from American Radiolabeled Chemicals Inc. (St. Louis, MO) via Hartman Analytics (Braunschweig, Germany). The syntheses of **6**,[38] **8**,[42] **15**,[39] **21**,[42] **25**,[27] **26**,[38] **29**[39] and **37**[38] were described elsewhere. Xanomeline (**35**)[72] and the pyrylium dye **9**[73] were prepared according to described procedures. Millipore water was used throughout for the preparation of buffers and HPLC eluents. Polypropylene reaction vessels (1.5 or 2 mL) with screw cap (Süd-Laborbedarf, Gauting, Germany) were used for the synthesis of the fluorescent ligands (**10**, **12**, **14**, **16-18**, **20**, **22**, **23**, **27**, **28** and **30**) and for the preparation and storage of stock solutions. NMR spectra were recorded on a Bruker Avance III HD 600 equipped with a cryogenic probe (14.1 T; 1H, 600 MHz) (Bruker, Karlsruhe, Germany). Abbreviations for the multiplicities of the signals are s (singlet), d (doublet), t (triplet), tt (triplet of triplet), m (multiplet), and brs (broad-singlet). High-resolution mass spectrometry (HRMS) analysis was performed with an Agilent 6540 UHD Accurate-Mass Q-TOF LC/MS system (Agilent Technologies, Santa Clara, CA) using an ESI source. Preparative HPLC was performed with a system from Knauer (Berlin, Germany) consisting of two K-1800 pumps and a K-2001 detector. A Kinetex-XB C18 (5 µm, 250 × 21 mm; Phenomenex, Aschaffenburg, Germany) was used as stationary phase at a flow rate of 15, 18 or 20 mL/min. Mixtures of acetonitrile and 0.1% or 0.2% aq TFA were used as mobile phase.

The detection wavelength was set to 220 nm throughout. The solvent of the collected fractions was removed by lyophilization using an Alpha 2-4 LD apparatus (Martin Christ, Osterode am Harz, Germany) equipped with a RZ 6 rotary vane vacuum pump (Vacuubrand, Wertheim, Germany). For compounds **10**, **12**, **14**, **16-18** and **20** analytical HPLC analysis (purity control) was performed on a system from Merck-Hitachi (Hitachi, Düsseldorf, Germany) composed of a L-6200-A pump, an AS-2000A autosampler, a L-4000A UV detector and a D-6000 interface. A Kinetex-XB C18, 5 μm, 250 × 4.6 mm (Phenomenex) was used as stationary phase at a flow rate of 0.8 mL/min. Mixtures of 0.1% aq TFA (A) and acetonitrile (B) were used as mobile phase (degassed by helium purging). The following linear gradient was applied: 0-30 min: A/B 95:5-15:85, 30-32 min: 15:85-5:95, 32-40 min: 5:95. The oven temperature was set to 25 °C and detection was performed at 220 nm. Analytical HPLC analysis of compounds **20** (chemical stability), **22**, **23**, **27**, **28** and **30** was performed with a system from Agilent Technologies composed of a 1290 Infinity binary pump equipped with a degasser, a 1290 Infinity autosampler, a 1290 Infinity thermostated column compartment, a 1260 Infinity diode array detector, and a 1260 Infinity fluorescence detector. A Kinetex-XB C18, 2.6 μm, 100 × 3 mm (Phenomenex) served as stationary phase at a flow rate of 0.5 mL/min. Mixtures of 0.04% aq TFA (A) and acetonitrile (B) were used as mobile phase. The following linear gradients were applied: compounds **22**, **23**, **27**, **28** and **30** (purity): 0-20 min: A/B 85:15-50:50, 20-22 min: 50:50-5:95, 22-28 min: 5:95; compounds **20** and **30** (chemical stabilities): 0-20 min: A/B 90:10-68:32, 20-22 min: 68:32-5:95, 22-26 min: 5:95. The oven temperature was set to 25 °C and detection was performed at 220 nm. Stock solutions (1, 5 or 10 mM) of fluorescent ligands were prepared in DMSO and were stored at −78 °C. Sigmacote (Sigma) was used for "siliconization" (coating) of glass and polypropylene reaction vessels used for the investigation of the chemical stabilities of **20**, **23**, **28** and **30**.

Compound Characterization. All target compounds (fluorescent ligands **10**, **12**, **14**, **16-18**, **20**, **22**, **23**, **27**, **28** and **30**) were characterized by HRMS and RP-HPLC analysis. Additionally, compounds **10**, **12**, **14**, **17**, **18**, **20**, **22**, **23**, **27**, **28** and **30** were characterized by ^{1}H-NMR (spectra shown in the Supporting Information). The HPLC purity of all fluorescent ligands amounted to ≥96% (220 nm) (chromatograms shown in the Supporting Information).

Screening for pan-assay interference compounds (PAINS). Screening of all target compounds for PAINS via the public tool http://zinc15.docking.org/patterns/home,[74] yielded no hits except for compounds **10** and **16**. In case of **10** and **16**, the *N*,*N*-dimethylaniline partial structure was identified as PAIN. The identities of **10** and **16** were proven by HRMS (in case of **10** additionally by ^{1}H-NMR) and both compounds exhibited a purity of 98%. Moreover, there are no reports on the *N*,*N*-dimethylaniline scaffold to exhibit high MR affinity as determined for **10** and **16**. Therefore, an interference in the radioligand competition binding assays by an impurity containing a *N*,*N*-dimethylaniline scaffold can be excluded.

Chemistry: experimental protocols and analytical data of compounds 10, 12, 14, 16-18, 20, 22, 23, 27, 28 and 30

4-((1*E*,3*E*)-4-(4-(Dimethylamino)phenyl)buta-1,3-dien-1-yl)-2,6-dimethyl-1-(4-(1-(2-oxo-2-(11-oxo-10,11-dihydro-5*H*-dibenzo[*b*,*e*][1,4]diazepin-5-yl)ethyl)piperidin-4-yl)butyl)pyridin-1-ium hydrotrifluoroacetate trifluoroacetate (10). The reaction was carried out in a 1.5-mL polypropylene reaction vessel equipped with a micro stir bar. Amine **8** (2.0 mg, 4.92 μmol) and triethylamine (5.0 mg, 6.8 μL, 49 μmol) were dissolved in anhydrous DMF (300 μL) followed by the addition of **9** (5.4 mg, 15 μmol) in anhydrous DMF (120 μL) and stirring at rt in the dark for 2 h. 10% aq TFA (corresponding to ca. 50 μmol of TFA) was added. Purification of the product by preparative HPLC (flow rate: 15 mL/min; gradient: 0-30

min: 0.1% aq TFA/acetonitrile 95:5-38:62, t_R = 17 min) afforded **10** as a red solid (0.91 mg, 21%). RP-HPLC (220 nm): 98% (t_R = 19.4 min, k = 5.8). ^{1}H-NMR (600 MHz, MeOH-d_4) (ratio of observed configurational isomers: ca 1.5:1): δ (ppm) 1.38-1.62 (m, 7H), 1.79-1.86 (m, 2H), 1.91-2.04 (m, 2H), 2.78 (s, 6H), 2.89-2.98 (m, 1H), 2.99-3.10 (m, 7H), 3.42-3.51 (m, 1H), 3.69-3.83 (m, 2H), 4.32-4.38 (m, 2H), 4.40 (d, *J* 17 Hz, 0.6H), 4.43 (d, *J* 17 Hz, 0.4H), 6.57 (d, *J* 16 Hz, 1H), 6.74-6.78 (m, 2H), 6.91-7.02 (m, 2H), 7.24-7.36 (m, 2H), 7.36-7.41 (m, 0.4H), 7.41-7.46 (m, 2H), 7.46-7.55 (m, 2.2H), 7.59-7.73 (m, 5H), 7.73-7.78 (m, 0.4H), 7.88-7.93 (m, 0.6H), 7.95-7.99 (m, 0.4H). HRMS (ESI): *m/z* $[M]^+$ calcd. for $[C_{43}H_{50}N_5O_2]^+$ 668.3959, found: 668.3963. $C_{43}H_{50}N_5O_2^+ \cdot C_4HF_6O_4^-$ (668.91 + 227.04).

2-((1*E*,3*E*)-5-((*E*)-3,3-Dimethyl-1-(6-oxo-6-((4-(1-(2-oxo-2-(11-oxo-10,11-dihydro-5*H*dibenzo[*b,e*][1,4]diazepin-5-yl)ethyl)piperidin-4-yl)butyl)amino)hexyl)indolin-2-ylidene)penta-1,3-dien-1-yl)-1,3,3-trimethyl-3*H*-indol-1-ium hydrotrifluoroacetate trifluoroacetate (12). Compound **12** was prepared from amine **8** (2.2 mg, 5.4 μmol) and **11** (2.4 mg, 3.6 μmol) according to the procedure for the synthesis of **10**, but DIPEA (4.7 mg, 6.3 μL, 36 μmol) was used instead of triethylamine. Purification by preparative HPLC (flow rate: 15 mL/min; gradient: 0-30 min: MeCN/0.1% aq TFA/acetonitrile 95:5-10:90, t_R = 14 min) afforded compound **12** as a dark blue solid (1.62 mg, 40%). RP-HPLC (220 nm): 97% (t_R = 25.9 min, k = 8.0). ^{1}H-NMR (600 MHz, MeOH-d_4) (ratio of observed configurational isomers: ca 1.5:1): δ (ppm) 1.27-1.35 (m, 4H), 1.39- 1.53 (m, 7H), 1.64-1.70 (m, 2H), 1.712 (s, 6H), 1.715 (s, 6H), 1.77-1.85 (m, 2H), 1.85-1.97 (m, 2H), 2.17 (t, *J* 7.4 Hz, 2H), 2.85-2.94 (m, 1H), 2.98-3.05 (m, 1H), 3.11 (t, *J* 7.2 Hz, 2H), 3.39-3.46 (m, 1H (interfering with the ^{13}C satellite of the solvent residual signal)), 3.61 (s, 3H), 3.67-3.80 (m, 2H), 4.08 (t, *J* 7.4 Hz, 2H), 4.37 (d, *J* 17 Hz, 0.6H), 4.41 (d, *J* 17 Hz, 0.4H), 6.26 (d, *J* 14 Hz, 2H), 6.60 (t, *J* 12 Hz, 1H), 7.23-7.35 (m, 6H), 7.36-7.43 (m, 2.4H), 7.45-7.54 (m, 4.2H), 7.59-7.65 (m, 1.4H), 7.66-7.70 (m, 0.6H), 7.72-7.76 (m, 0.4H), 7.88-7.92 (m, 0.6H), 7.95-7.88 (m, 0.4H), 8.19-8.27 (m, 2H). HRMS

(ESI): *m/z* $[M]^+$ calcd. for $[C_{56}H_{67}N_6O_3]^+$ 871.5269, found: 871.5265. $C_{56}H_{67}N_6O_3^+ \cdot C_4HF_6O_4^-$ (872.19 + 227.04).

4-(2-((1*E*,3*E*)-5-((*E*)-3,3-Dimethyl-1-(6-oxo-6-((4-(1-(2-oxo-2-(11-oxo-10,11-dihydro-5*H*dibenzo[*b*,*e*][1,4]diazepin-5-yl)ethyl)piperidin-4-yl)butyl)amino)hexyl)indolin-2-ylidene)penta-1,3-dien-1-yl)-3,3-dimethyl-3*H*-indol-1-ium-1-yl)butane-1-sulfonate hydrotrifluoroacetate (14). Compound **14** was prepared from amine **8** (1.9 mg, 4.7 µmol) and **13** (2.2 mg, 3.1 µmol) according to the procedure for the synthesis of **10**, but DIPEA (4.05 mg, 5.5 µL, 31 µmol) was used instead of triethylamine. Purification by preparative HPLC (conditions as used for **12**, t_R = 15 min) afforded compound **14** as a dark blue solid (1.43 mg, 37%). RP-HPLC (220 nm): 96% (t_R = 24.2 min, k = 7.4). ^{1}H-NMR (600 MHz, MeOH-d_4) (ratio of observed configurational isomers: ca 1.5:1): δ (ppm) 1.28-1.36 (m, 4H), 1.41-1.55 (m, 7H), 1.63-1.76 (m, 14H), 1.77-1.89 (m, 3H), 1.90-2.01 (m, 5H), 2.18 (t, *J* 7.4 Hz, 2H), 2.85-2.96 (m, 3H), 3.00-3.08 (m, 1H), 3.10-3.16 (m, 2H), 3.39-3.47 (m, 1H (interfering with the ^{13}C satellite of the solvent residual signal)), 3.67-3.79 (m, 2H), 4.03-4.16 (m, 4H), 4.37 (d, *J* 17 Hz, 0.6H), 4.43 (d, *J* 17 Hz, 0.4H), 6.23-6.28 (m, 1H), 6.31-6.37 (m, 1H), 6.59-6.67 (m, 1H), 7.22-7.29 (m, 3.6H), 7.29-7.43 (m, 4.6H), 7.43-7.55 (m, 4.4H), 7.59-7.68 (m, 2H), 7.71-7.76 (m, 0.4H), 7.86-7.90 (m, 0.6H), 7.93-7.97 (m, 0.4H), 8.17-8.26 (m, 2H). HRMS (ESI): *m/z* $[M+H]^+$ calcd. for $[C_{59}H_{73}N_6O_6S]^+$ 993.5307, found: 993.5317. $C_{59}H_{72}N_6O_6S \cdot C_2HF_3O_2$ (993.32 + 114.02).

4-((1*E*,3*E*)-4-(4-(Dimethylamino)phenyl)buta-1,3-dien-1-yl)-2,6-dimethyl-1-(2-(4-(4-(1-(2-oxo-2-(11-oxo-10,11-dihydro-5*H*-dibenzo[*b*,*e*][1,4]diazepin-5-yl)ethyl)piperidin-4-yl)butyl)piperazin-1-yl)ethyl)pyridin-1-ium tris(hydrotrifluoroacetate) trifluoroacetate (16). Compound **16** was prepared from amine **15** (3.0 mg, 3.1 µmol) and **9** (3.6 mg, 9.9 µmol) according to the procedure for the synthesis of **10**. Triethylamine: 5.36 mg, 7.4 µL, 52.9 µmol. Purification of the product by preparative HPLC (flow rate: 15 mL/min; gradient: 0-30 min:

0.1% aq TFA/acetonitrile 85:15-38:62, t_R = 12 min) afforded **16** as a red solid (1.31 mg, 34%). RP-HPLC (220 nm): 98% (t_R = 16.6 min, k = 4.8); HRMS (ESI): *m/z* $[M]^+$ calcd. for $[C_{49}H_{62}N_7O_2]^+$ 780.4960, found: 780.4961. $C_{49}H_{62}N_7O_2^+ \cdot C_8H_3F_{12}O_8^-$ (781.08 + 455.09).

2-((1*E*,3*E*)-5-((*E*)-3,3-Dimethyl-1-(6-oxo-6-((2-(4-(4-(1-(2-oxo-2-(11-oxo-10,11-dihydro-5*H*dibenzo[*b,e*][1,4]diazepin-5-yl)ethyl)piperidin-4-yl)butyl)piperazin-1-yl)ethyl)amino)hexyl)indolin-2-ylidene)penta-1,3-dien-1-yl)-1,3,3-trimethyl-3*H*-indol-1-ium tris(hydrotrifluoroacetate) trifluoroacetate (17). Compound **17** was prepared from amine **15** (5.8 mg, 5.95 µmol) and **11** (3.0 mg, 4.5 µmol) according to the procedure for the synthesis of **10**, but DIPEA (5.9 mg, 7.9 µL, 45 µmol) was used instead of triethylamine and the reaction time was 1 h instead of 2 h. Purification by preparative HPLC (conditions as used for **12**, t_R = 19 min) afforded the product as a dark blue solid (2.06 mg, 31%). RP-HPLC (220 nm): 97% (t_R = 21.9 min, k = 6.6). ^{1}H-NMR (600 MHz, MeOH-d_4) (ratio of observed configurational isomers: ca 1.5:1): δ (ppm) 1.31-1.41 (m, 4H), 1.42-1.56 (m, 5H), 1.64-1.75 (m, 16H), 1.78-1.85 (m, 2H), 1.86-1.99 (m, 2H), 2.21 (t, *J* 7.5 Hz, 2H), ca. 2.5-3.1 (brs, 4H (interfering with the next three listed signals)), 2.61-2.67 (m, 2H), 2.87-2.95 (m, 1H), 3.00-3.07 (m, 3H), ca. 3.1-3.5 (brs, 4H (interfering with the next two listed signals)), 3.31-3.34 (m, 2H (interfering with the solvent residual signal)), 3.41-3.48 (m, 1H (interfering with the ^{13}C satellite of the solvent residual signal)), 3.62 (s, 3H), 3.68-3.81 (m, 2H), 4.09 (t, *J* 7.4 Hz, 2H), 4.39 (d, *J* 17 Hz, 0.6H), 4.42 (d, *J* 17 Hz, 0.4H), 6.26 (d, *J* 14 Hz, 2H), 6.57-6.64 (m, 1H), 7.23-7.35 (m, 6H), 7.36-7.43 (m, 2.4H), 7.45-7.55 (m, 4.2H), 7.59-7.66 (m, 1.4H), 7.66-7.71 (m, 0.6H), 7.72-7.77 (m, 0.4H), 7.88-7.92 (m, 0.6H), 7.95-7.98 (m, 0.4H), 8.20-8.27 (m, 2H). HRMS (ESI): *m/z* $[M]^+$ calcd. for $[C_{62}H_{79}N_8O_3]^+$ 983.6270, found: 983.6275. $C_{62}H_{79}N_8O_3^+ \cdot C_8H_3F_{12}O_8^-$ (984.37 + 455.09).

4-(2-((1*E*,3*E*)-5-((*E*)-3,3-Dimethyl-1-(6-oxo-6-((2-(4-(4-(1-(2-oxo-2-(11-oxo-10,11-dihydro-5*H*-dibenzo[*b*,*e*][1,4]diazepin-5-yl)ethyl)piperidin-4-yl)butyl)piperazin-1-yl)ethyl)amino)hexyl)indolin-2-ylidene)penta-1,3-dien-1-yl)-3,3-dimethyl-3*H*-indol-1-ium-1-yl)butane-1-sulfonate tris(hydrotrifluoroacetate) (18). Compound **18** was prepared from amine **15** (3.7 mg, 3.8 μmol) and **13** (2.4 mg, 3.4 μmol) according to the procedure for the synthesis of **10**, but DIPEA (4.4 mg, 5.9 μL, 34 μmol) was used instead of triethylamine and the reaction time was 1 h instead of 2 h. Purification by preparative HPLC (conditions as used for **12**, t_R = 18 min) afforded the product as a dark blue solid (1.59 mg, 30%). RP-HPLC (220 nm): 96% (t_R = 21.3 min, k = 6.4). ^{1}H-NMR (600 MHz, MeOH-d_4) (ratio of observed configurational isomers: ca 1.5:1): δ (ppm) 1.31-1.62 (m, 9H), 1.65-1.77 (m, 16H), 1.78-1.85 (m, 2H), 1.86-2.01 (m, 6H), 2.23 (t, *J* 7.3 Hz, 2H), ca. 2.4-3.6 (brs, 8H (interfering with the next five listed signals)), 2.70 (brs, 2H), 2.86-2.97 (m, 3H), 3.01-3.10 (m, 3H), 3.36 (brs, 2H), 3.40-3.46 (m, 1H (interfering with the ^{13}C satellite of the solvent residual signal)), 3.67-3.81 (m, 2H), 4.09 (t, *J* 7.6 Hz, 2H), 4.13 (brs, 2H), 4.38 (d, *J* 17 Hz, 0.6H), 4.42 (d, *J* 17 Hz, 0.4H), 6.27 (d, *J* 14 Hz, 1H), 6.34 (d, *J* 14 Hz, 1H), 6.61-6.68 (m, 1H), 7.23-7.30 (m, 3.6H), 7.30-7.35 (m, 2.4H), 7.35-7.42 (m, 2.4H), 7.45-7.55 (m, 4.2H), 7.59-7.70 (m, 2H), 7.72-7.76 (m, 0.4H), 7.88-7.91 (m, 0.6H), 7.95-7.98 (m, 0.4H), 8.20-8.27 (m, 2H). HRMS (ESI): *m/z* $[M+H]^+$ calcd. for $[C_{65}H_{85}N_8O_6S]^+$ 1105.6307, found: 1105.6309. $C_{65}H_{84}N_8O_6S \cdot C_6H_3F_9O_6$ (1105.50 + 342.07).

4-(2-((1*E*,3*E*)-5-((*E*)-3,3-dimethyl-1-(6-oxo-6-((2-(4-(4-(1-(2-oxo-2-(11-oxo-10,11-dihydro-5*H*-dibenzo[*b*,*e*][1,4]diazepin-5-yl)ethyl)piperidin-4-yl)butyl)piperazin-1-yl)ethyl)amino)hexyl)-5-sulfoindolin-2-ylidene)penta-1,3-dien-1-yl)-3,3-dimethyl-3*H*-indol-1-ium-1-yl)butane-1-sulfonate bis(hydrotrifluoroacetate) (20). Compound **20** was prepared from amine **15** (4.5 mg, 4.6 μmol) and **19** (2.3 mg, 2.9 μmol) according to the procedure for the synthesis of **10**, but DIPEA (4.2 mg, 5.7 μL, 33 μmol) was used instead of triethylamine and the reaction time was 1 h instead of 2 h. Purification by preparative HPLC

(conditions as used for **12**, t_R = 15 min) afforded the product as a dark blue solid (1.45 mg, 30%). RP-HPLC (220 nm): 96% (t_R = 18.2 min, k = 18.8). ^{1}H-NMR (600 MHz, MeOH-d_4) (ratio of observed configurational isomers: ca 1.5:1): δ (ppm) 1.34-1.56 (m, 8H), 1.59-1.78 (m, 17H), 1.79-1.86 (m, 2H), 1.90-2.04 (m, 6H), 2.18 (t, *J* 6.8 Hz, 2H), 2.36 (brs, 2H), ca. 2.4 (brs, 1H), 2.80-3.14 (m, 9H), ca. 3.14-3.60 (brs, 4H (interfering with the next two listed signals)), 3.17-3.22 (m, 2H (interfering with ^{13}C satellite of the solvent residual signal)), 3.41-3.48 (m, 1H (interfering with the ^{13}C satellite of the solvent residual signal)), 3.70-3.83 (m, 2H), 4.07 (t, *J* 6.8 Hz, 2H), 4.22 (t, *J* 7.5 Hz, 2H), 4.38 (d, *J* 17 Hz, 0.6H), 4.43 (d, *J* 17 Hz, 0.4H), 6.21 (d, *J* 13 Hz, 1H), 6.45 (d, *J* 14 Hz, 1H), 6.64-6.71 (m, 1H), 7.24-7.35 (m, 4H), 7.36-7.40 (m, 0.4H), 7.40-7.48 (m, 2.6H), 7.48-7.55 (m, 2.6H), 7.59-7.70 (m, 2H), 7.72-7.76 (m, 0.4H), 7.81-7.86 (m, 2H), 7.88-7.91 (m, 0.6H), 7.95-7.98 (m, 0.4H), 8.21 (t, *J* 13 Hz, 1H), 8.29 (t, *J* 13 Hz, 1H). HRMS (ESI): *m/z* $[M+H]^+$ calcd. for $[C_{65}H_{85}N_8O_9S_2]^+$ 1185.5875, found: 1185.5896. $C_{65}H_{84}N_8O_9S_2 \cdot C_4H_2F_6O_4$ (1185.55 + 228.05).

4-(2-((1*E*,3*E*)-5-((*E*)-3,3-dimethyl-1-(6-oxo-6-((2-(3-(1-(4-(1-(2-oxo-2-(11-oxo-10,11-dihydro-5*H*-dibenzo[*b,e*][1,4]diazepin-5-yl)ethyl)piperidin-4-yl)butyl)-1*H*-imidazol-4-yl)propanamido)ethyl)amino)hexyl)indolin-2-ylidene)penta-1,3-dien-1-yl)-3,3-dimethyl-3*H*-indol-1-ium-1-yl)butane-1-sulfonate bis(hydrotrifluoroacetate) (22). The reaction was carried out in a 1.5-mL polypropylene reaction vessel equipped with a micro stir bar. Amine **21** (7.0 mg, 7.6 μmol) and DIPEA (6.6 mg, 9.0 μL, 51 μmol) were dissolved in anhydrous DMF (50 μL) followed by the addition of **13** (3.6 mg, 5.1 μmol) in anhydrous DMF (50 μL) and stirring was continued at rt in the dark for 1 h. 10% aq TFA (100 μL) was added and purification by preparative HPLC (flow rate: 18 mL/min; gradient: 0-25 min: 0.1% aq TFA/acetonitrile 85:15-55:45, t_R = 18 min) afforded **22** as a dark blue fluffy solid (2.4 mg, 34%). RP-HPLC (220 nm): 99% (t_R = 14.5, k = 14.8). ^{1}H-NMR (600 MHz, MeOH-d_4) (ratio of observed configurational isomers: ca 1.5:1): δ (ppm) 1.32 (brs, 4H), 1.41-1.56 (m, 5H), 1.64-1.76 (m,

14H), 1.77-1.89 (m, 5H), 1.96 (brs, 5H), 2.20 (t, *J* 7.4 Hz, 2H), 2.57 (t, *J* 7.1 Hz, 2H), 2.87-2.98 (m, 5H), 3.01-3.07 (m, 1H), 3.24 (s, 4H), 3.41-3.47 (m, 1H (interfering with the ^{13}C satellite of the solvent residual signal)), 3.67-3.81 (m, 2H), 4.09 (t, *J* 7.4 Hz, 2H), 4.11-4.19 (m, 4H), 4.38 (d, *J* 17 Hz, 0.6H), 4.43 (d, *J* 17 Hz, 0.4H), 6.23-6.28 (m, 1H), 6.32-6.37 (m, 1H), 6.59-6.67 (m, 1H), 7.23-7.29 (m, 3.8H), 7.30-7.34 (m, 2.2H), 7.34-7.43 (m, 3.4H), 7.44-7.55 (m, 4.2H), 7.59-7.68 (m, 2H), 7.71-7.76 (m, 0.4H), 7.87-7.90 (m, 0.6H), 7.94-7.97 (m, 0.4H), 8.19-8.26 (m, 2H), 8.78 (brs, 1H). HRMS (ESI): *m/z* $[M+2H]^{2+}$ calcd. for $[C_{67}H_{85}N_9O_7S]^{2+}$ 579.8141, found: 579.8153. $C_{67}H_{83}N_9O_7S \cdot C_4H_2F_6O_4$ (1158.52 + 228.05).

4-(2-((1*E*,3*E*)-5-((E)-3,3-dimethyl-1-(6-oxo-6-((2-(3-(1-(4-(1-(2-oxo-2-(11-oxo-10,11-dihydro-5*H*-dibenzo[*b,e*][1,4]diazepin-5-yl)ethyl)piperidin-4-yl)butyl)-1*H*-imidazol-4-yl)propanamido)ethyl)amino)hexyl)-5-sulfoindolin-2-ylidene)penta-1,3-dien-1-yl)-3,3-dimethyl-3*H*-indol-1-ium-1-yl)butane-1-sulfonate hydrotrifluoroacetate (23). Compound **23** was prepared from amine **21** (3.2 mg, 3.5 μmol) and **19** (1.9 mg, 2.3 μmol) according to the procedure for the synthesis of **22**. DIPEA: 3.0 mg, 4.0 μL, 23 μmol. Purification by preparative HPLC (conditions as used for **22**, t_R = 14 min) afforded **23** as a dark blue fluffy solid (1.4 mg, 41%). RP-HPLC (220 nm): 98% (t_R = 10.0, k = 9.9). ^{1}H-NMR (600 MHz, MeOH-d_4) (ratio of observed configurational isomers: ca 1.5:1): δ (ppm) 1.31 (brs, 4H), 1.36-1.55 (m, 5H), 1.62-1.68 (m, 2H), 1.69-1.72 (m, 6H), 1.73 (s, 6H), 1.77-1.86 (m, 5H), 1.88-1.98 (m, 3H), 2.01 (brs, 2H), 2.16 (t, *J* 7.1 Hz, 2H), 2.55 (t, *J* 7.1 Hz, 2H), 2.88-2.97 (m, 5H), 3.01-3.08 (m, 1H), 3.15 (s, 4H), 3.40-3.46 (m, 1H (interfering with the ^{13}C satellite of the solvent residual signal)), 3.69-3.81 (m, 2H), 4.06 (t, *J* 6.7 Hz, 2H), 4.16 (t, *J* 7.2 Hz, 2H), 4.21 (t, *J* 7.0 Hz, 2H), 4.39 (d, *J* 17 Hz, 0.6H), 4.45 (d, *J* 17 Hz, 0.4H), 6.18-6.23 (m, 1H), 6.49 (d, *J* 14 Hz, 1H), 6.63-6.69 (m, 1H), 7.21-7.28 (m, 1.8H), 7.30-7.34 (m, 2.2H), 7.35-7.38 (m, 0.4H), 7.38-7.48 (m, 3.6H), 7.48-7.55 (m, 2.6H), 7.59-7.63 (m, 0.4H), 7.63-7.69 (m, 1.6H), 7.72-7.76 (m, 0.4H), 7.80-7.86 (m, 2H), 7.87-7.91 (m, 0.6H), 7.94-7.97 (m, 0.4H), 8.20 (t, *J* 13 Hz, 1H), 8.28 (t, *J* 13 Hz, 1H), 8.77 (brs,

1H). HRMS (ESI): *m/z* $[M+2H]^{2+}$ calcd. for $[C_{67}H_{85}N_9O_{10}S_2]^{2+}$ 619.7925, found: 619.7941. $C_{67}H_{83}N_9O_{10}S_2 \cdot C_2HF_3O_2$ (1238.58 + 114.02).

4-(2-((1*E*,3*E*)-5-((*E*)-1-(6-((3,5-bis((2-(3-(1-(4-(1-(2-oxo-2-(11-oxo-10,11-dihydro-5*H*-dibenzo[*b,e*][1,4]diazepin-5-yl)ethyl)piperidin-4-yl)butyl)-1*H*-imidazol-4-yl)propanamido)ethyl)carbamoyl)benzyl)amino)-6-oxohexyl)-3,3-dimethylindolin-2-ylidene)penta-1,3-dien-1-yl)-3,3-dimethyl-3*H*-indol-1-ium-1-yl)butane-1-sulfonate tetrakis(hydrotrifluoroacetate) (27). Compound **27** was prepared from amine **26** (6.0 mg, 4.6 μmol) and **13** (2.2 mg, 3.1 μmol) according to the procedure for the synthesis of **22**. DIPEA: 4.0 mg, 5.4 μL, 31 μmol. Purification by preparative HPLC (flow rate: 18 mL/min; gradient: 0-25 min: 0.1% aq TFA/acetonitrile 85:15-40:60, t_R = 16 min) afforded **27** as a dark blue fluffy solid (2.6 mg, 36%). RP-HPLC (220 nm): 99% (t_R = 13.3, k = 13.5). ^{1}H-NMR (600 MHz, MeOH-d_4) (ratio of observed configurational isomers: ca 1.5:1): δ (ppm) 1.30 (brs, 8H), 1.38-1.56 (m, 8H), 1.69 (s, 6H), 1.71 (s, 6H), 1.72-1.77 (m, 2H), 1.78-1.88 (m, 8H), 1.88-1.97 (brs, 6H), 2.32 (t, *J* 7.1 Hz, 2H), 2.58 (t, *J* 7.1 Hz, 4H), 2.85-2.98 (m, 8H), 3.03 (brs, 2H), 3.37 (t, *J* 6.0 Hz, 4H), 3.43 (brs, 1H (interfering with the ^{13}C satellite of the solvent residual signal)), 3.44-3.49 (m, 5H), 3.66-3.82 (m, 4H), 4.06-4.16 (m, 8H), 4.39 (d, *J* 17 Hz, 1.2H), 4.43 (d, *J* 17 Hz, 0.8H), 4.46 (s, 2H), 6.26 (d, *J* 14 Hz, 2H), 6.51 (t, *J* 12 Hz, 1H), 7.23-7.29 (m, 5H), 7.29-7.34 (m, 3H), 7.35 (brs, 2H), 7.36-7.42 (m, 2.6H), 7.44-7.52 (m, 6.6H), 7.59-7.68 (m, 4H), 7.71-7.75 (m, 0.8H), 7.87-7.90 (m, 1.2H), 7.91 (brs, 2H), 7.94-7.97 (m, 0.8H), 8.16-8.24 (m, 3H), 8.75 (brs, 2H). HRMS (ESI): *m/z* $[M+4H]^{4+}$ calcd. for $[C_{108}H_{133}N_{17}O_{12}S]^{4+}$ 473.0005, found: 473.0016. $C_{108}H_{129}N_{17}O_{12}S \cdot C_8H_4F_{12}O_8$ (1889.39 + 456.09).

4-(2-((1*E*,3*E*)-5-((*E*)-1-(6-((3,5-Bis((2-(3-(1-(4-(1-(2-oxo-2-(11-oxo-10,11-dihydro-5*H*-dibenzo[*b,e*][1,4]diazepin-5-yl)ethyl)piperidin-4-yl)butyl)-1*H*-imidazol-4-yl)propanamido)ethyl)carbamoyl)benzyl)amino)-6-oxohexyl)-3,3-dimethyl-5-

sulfoindolin-2-ylidene)penta-1,3-dien-1-yl)-3,3-dimethyl-3*H*-indol-1-ium-1-yl)butane-1-sulfonate tris(hydrotrifluoroacetate) (28). Compound **28** was prepared from amine **26** (6.0 mg, 4.6 μmol) and **19** (7.6 mg, 3.1 μmol) according to the procedure for the synthesis of **22**. DIPEA: 4.0 mg, 5.4 μL, 31 μmol. Purification by preparative HPLC (conditions as used for **22**, t_R = 15 min) afforded **28** as a dark blue fluffy solid (2.9 mg, 26%). RP-HPLC (220 nm): 99% (t_R = 10.4, k = 10.3). ^{1}H-NMR (600 MHz, MeOH-d_4) (ratio of observed configurational isomers: ca 1.5:1): δ (ppm) 1.30 (brs, 8H), 1.37-1.55 (m, 8H), 1.65-1.74 (m, 14H), 1.76-1.88 (m, 8H), 1.88-1.97 (m, 4H), 2.00 (brs, 2H), 2.28 (t, *J* 6.8 Hz, 2H), 2.58 (t, *J* 7.1 Hz, 4H), 2.86-2.97 (m, 8H), 3.04 (brs, 2H), 3.35-3.39 (m, 4H), 3.43 (brs, 1H (interfering with the ^{13}C satellite of the solvent residual signal)), 3.44-3.48 (m, 5H), 3.67-3.82 (m, 4H), 4.04 (brs, 2H), 4.11 (t, *J* 7.2 Hz, 4H), 4.21 (t, *J* 7.1 Hz, 2H), 4.32 (s, 2H), 4.39 (d, *J* 17 Hz, 1.2H), 4.44 (d, *J* 17 Hz, 0.8H), 6.17 (d, *J* 13 Hz, 1H), 6.46 (d, *J* 14 Hz, 1H), 6.55-6.63 (m, 1H), 7.17 (d, *J* 8.3 Hz, 1H), 7.23-7.28 (m, 1.6H), 7.29-7.34 (m, 3.4H), 7.34-7.39 (m, 2.6H), 7.39-7.54 (m, 7.6H), 7.58-7.68 (m, 4H), 7.71-7.76 (m, 1.8H), 7.84 (brs, 1H), 7.87-7.91 (m, 3.2H), 7.93-7.97 (m, 0.8H), 8.12-8.20 (m, 2H), 8.26 (t, *J* 13 Hz, 1H), 8.74 (brs, 2H). HRMS (ESI): *m/z* $[M+3H]^{3+}$ calcd. for $[C_{108}H_{132}N_{17}O_{15}S_2]^{3+}$ 656.9838, found: 656.9851. $C_{108}H_{129}N_{17}O_{15}S_2 \cdot C_6H_3F_9O_6$ (1969.44 + 342.07).

4-(2-((1*E*,3*E*)-5-((*E*)-3,3-dimethyl-1-(6-oxo-6-((3-((2-(4-(2-oxo-2,3-dihydro-1*H*-benzo[*d*]imidazol-1-yl)-[1,4'-bipiperidin]-1'-yl)ethyl)carbamoyl)-5-((2-(4-(4-(1-(2-oxo-2-(11-oxo-10,11-dihydro-5*H*-dibenzo[*b*,*e*][1,4]diazepin-5-yl)ethyl)piperidin-4-yl)butyl)piperazin-1-yl)ethyl)carbamoyl)benzyl)amino)hexyl)-5-sulfoindolin-2-ylidene)penta-1,3-dien-1-yl)-3,3-dimethyl-3*H*-indol-1-ium-1-yl)butane-1-sulfonate tetrakis(hydrotrifluoroacetate) (30). Compound **30** was prepared from amine **29** (5.0 mg, 4.9 μmol) and **19** (2.6 mg, 3.3 μmol) according to the procedure used for the synthesis of **22**. DIPEA: 4.3 mg, 6.0 μL, 33 μmol. Purification by preparative HPLC (conditions as used for **22**,

t_R = 14 min) afforded **30** as a dark blue fluffy solid (2.3 mg, 34%). RP-HPLC (220 nm): 97% (t_R = 9.4, k = 9.2). ^{1}H-NMR (600 MHz, MeOH-d_4) (ratio of observed configurational isomers: ca 1.5:1): δ (ppm) 1.30-1.60 (m, 9H), 1.64-1.77 (m, 16H), 1.77-1.84 (m, 2H), 1.86-1.98 (m, 4H), 1.98-2.05 (m, 2H), ca. 2.0-4.3 (brs, 8H (interfering with the next 16 listed signals)), 2.09-2.15 (m, 2H), 2.24-2.35 (m, 4H), 2.43-2.51 (m, 2H), 2.67 (t, *J* 6.2 Hz, 2H), 2.82-2.91 (m, 4H), 2.91-2.98 (m, 1H), 3.01-3.09 (m, 3H), 3.13-3.23 (brs, 2H (interfering with the ^{13}C satellite of the solvent residual signal)), 3.32-3.38 (m, 2H), 3.39-3.47 (m, 3H), 3.50 (t, *J* 6.6 Hz, 2H), 3.66 (brs, 1H), 3.69-3.83 (m, 6H), 3.98 (brs, 2H), 4.02 (t, *J* 7.1 Hz, 2H), 4.22 (t, *J* 7.3 Hz, 2H), 4.36 (brs, 2H), 4.39 (d, *J* 17 Hz, 0.6H), 4.44 (d, *J* 17 Hz, 0.4H), 4.59 (tt, *J* 12.3, 4.3 Hz, 1H), 6.19 (d, *J* 13 Hz, 1H), 6.48 (d, *J* 14 Hz, 1H), 6.63 (t, *J* 12 Hz, 1H), 7.02-7.09 (m, 3H), 7.14 (d, *J* 8.3 Hz, 1H), 7.24-7.35 (m, 4H), 7.35-7.54 (m, 5.6H), 7.59-7.70 (m, 3H), 7.72-7.76 (m, 0.4H), 7.81 (brs, 1H), 7.88-7.91 (m, 0.6H), 7.93 (brs, 1H), 7.95-7.98 (m, 1.4H), 8.14 (t, *J* 13 Hz, 1H), 8.21 (brs, 1H), 8.25 (t, *J* 13 Hz, 1H). HRMS (ESI): *m/z* $[M+3H]^{3+}$ calcd. for $[C_{93}H_{121}N_{14}O_{12}S_2]^{3+}$ 563.2904, found: 563.2916. $C_{93}H_{118}N_{14}O_{12}S_2 \cdot C_8H_4F_{12}O_8$ (1688.17 + 456.09).

Investigation of the chemical stability. The chemical stabilities of **20**, **23**, **28** and **30** were investigated in PBS pH 7.4 at 22 ± 1 °C using siliconized (Sigmacote, Sigma) flat-bottom glass tubes (8.2 × 40 mm; Altmann Analytik, Munich, Germany) in case of **20** and **23**, and different vessel materials (polypropylene, siliconized glass (the same type as for **20** and **23**) or coated ("siliconized") polypropylene) for **28** and **30**. The incubation was started by the addition of 10 µL of 1 mM solution of the fluorescent ligand in DMSO to PBS (90 µL) to yield a final concentration of 100 µM. After 0, 24 and 48 h, aliquots (20 µL) were taken and added to 1% aq TFA/acetonitrile (8:2 v/v) (20 µL). The resulting solutions were analyzed by RP-HPLC (analytical HPLC system and conditions see general experimental conditions; t_R: 18.2 min (**20**), 10.3 min (**23**), 10.4 min (**28**), 18.0 min (**30**)).

Determination of Fluorescence Quantum Yields. The determination of the fluorescence quantum yields of the fluorescently labeled ligands **16-18**, **20**, **22**, **23** and **28**, dissolved in PBS or PBS containing 1% BSA, was performed with a Cary Eclipse spectrofluorimeter and a Cary 100 UV/VIS photometer (Varian Inc., Mulgrave, Victoria, Australia) as described previously with minor modifications.[12] All spectra were recorded using acryl cuvettes (10 × 10 mm, Ref. 67.755, Sarstedt, Nümbrecht, Germany). Fluorescence spectra were recorded at the slit adjustments (excitation/emission) 10/5 nm and 10/10 nm and resulting quantum yields were averaged. Table 7 provides an overview of the used concentrations of the fluorescent ligands and the applied excitation wavelengths. The concentration of cresyl violet perchlorate in EtOH was 2 μM. Fluorescence spectra of cresyl violet perchlorate were recorded using an excitation wavelength of 575 nm.

Table 7. Fluorescent ligand concentrations and excitation wavelengths used for the determination of fluorescence quantum yields.

compd.	concentration [μM]		λ_{ex} [nm]	
	PBS	PBS + 1% BSA	PBS	PBS + 1% BSA
16	15	12	445	470
17	5	5	600	610
18	3	2	610	620
20	2	2	610	610
22	2.5	2.5	605	610
23	2.5	2.5	604	609
28	2.5	2.5	617	613

Cell culture. CHO-K9 cells, stably transfected with the DNA of human muscarinic receptors M_1-M_5 (obtained from Missouri S&T cDNA Resource Center; Rolla, MO) were cultured in HAM's F12 medium supplemented with fetal calf serum (Biochrom, Berlin, Germany) (10%) and G418 (Biochrom) (750 μg/mL).

IP1 accumulation assays. The M_2R IP1 accumulation assay was performed as described elsewhere.[38] In addition to the previously described conditions used for the investigation of M_2R antagonism (preincubation of the cells with antagonist at 37 °C for 30 min followed by addition of CCh (0.3 μM) and continuation of the incubation at 37 °C for 60 min), cells were preincubated with **20** or **23** at 22 °C for 180 min followed by addition of CCh (final concentration: 0.3 μM) and continuation of the incubation at 37 °C for 90 min.

The M_4R IP1 accumulation assay was essentially performed as the previously described M_2R IP1 accumulation assay[38] using the cDNA of the human M_4R (Missouri S&T cDNA Resource Center) to prepare transiently transfected HEK-hM_4-Gα_{qi5}-$_{HA}$ cells. To investigate M_2R antagonism, cells were preincubated with the antagonist at rt for 180 min followed by addition of CCh (final concentration: 0.1 μM) and continuation of the incubation at 37 °C for 90 min.

Radioligand competition binding. Equilibrium competition binding experiments with [^{3}H]NMS were performed at intact CHO-hM_xR cells (x = 1-5) as described previously,[42] but the total volume per well was 200 μL, i.e., in case of total binding, wells were filled with 180 μL of L15 medium followed by the addition of L15 medium (20 μL) containing [^{3}H]NMS (10-fold concentrated). To determine unspecific binding and the effect of a compound of interest on [^{3}H]NMS equilibrium binding, wells were filled with 160 μL of L15 medium followed by the addition of L15 medium (20 μL) containing **31** or the compound of interest (10-fold concentrated) and L15 medium (20 μL) containing [^{3}H]NMS (10-fold concentrated). Samples containing fluorescent ligand were incubated in the dark.

Flow cytometry. All flow cytometric binding studies (fluorescent ligands **18**, **20**, **23**, **28** and **30**) were performed with a FACSCalibur flow cytometer (Becton Dickinson, Heidelberg, Germany) (saturation and competition binding) or with a FACSCanto II (Becton Dickinson)

(association and dissociation experiments), both equipped with an argon laser (488 nm) and a red diode laser (635 and 640 nm, respectively). Settings for forward and sideward scatter were: FSC: E-1, SSC: 280 V (FACSCalibur), or FSC: 0 V, SSC: 252 V (FACSCantoII). Fluorescence was recorded in channel FL-4 (excitation: 635 nm, emission: 661 ± 9 nm, gain: 700-800 V) and in cannel APC-A (excitation: 640 nm, emission: 660 ± 10 nm, gain: 510-540 V), respectively. Measurements were stopped after counting of 10,000 (FACSCanto II, flow rate: medium) or 20,000 (FACSCalibur, flow rate: high) gated events. Samples were prepared and incubated (22 °C, in the dark) in 1.5 mL polypropylene reaction vessels (Sarstedt, Nümbrecht, Germany) or 50 mL polypropylene vessels (VWR International, Radnor, PA). All experiments were performed in duplicate. Cells were seeded in 175-cm^2 culture flasks 5-6 days prior to the experiment. On the day of the experiment, cells were treated with trypsin, suspended in culture medium and centrifuged. The cell pellet was re-suspended in Leibovitz's L15 culture medium (Gibco, Life Technologies, Darmstadt, Germany) supplemented with 1% BSA (in the following referred to as L15 medium). The cell density was adjusted to 0.9-1.1 × 10^6 cells/mL. For saturation (**18**, **20**, **23**, **28**, **30**) and competition (**20**) binding experiments, 1.5 mL reaction vessels were prefilled with 490 µL of the cell suspension. For total binding, DMSO/H_2O (1:1 v/v) (5 µL) and DMSO/H_2O (1:1 v/v) (5 µL), containing the fluorescent ligand (100-fold concentrated), were added. To determine unspecific binding and in case of competition binding, DMSO/H_2O (1:1 v/v) (5 µL), containing atropine (**31**) (100-fold concentrated) and the compound of interest (100-fold concentrated), respectively, and DMSO/H_2O (1:1 v/v) (5 µL), containing the fluorescent ligand (100-fold concentrated), were added. For saturation binding experiments at the M_2R the following final concentrations of fluorescent ligands were applied: 0.1-15 nM (**18**), 0.1-10 nM (**20**), 0.005-50 nM (**23**), 0.15-80 nM (**28**) and 0.04-20 nM (**30**). For saturation binding studies at the M_1R and M_4R, compound **20** was applied at final concentrations of 0.15-80 nM. For competition binding experiments with **20**, the final concentration of **20** was 1 or 20 nM. Unspecific binding was determined in the presence of **31**

at 500-fold access to the fluorescent ligands. Samples were incubated at 22 °C in the dark under gentle shaking for 2 h.

For association experiments with **20** (1 nM), **23** (5 nM) and **28** (3.5 nM) at CHO-hM_2R cells, 50 mL reaction vessels were prefilled with 5 mL (total binding) or 2.5 mL (unspecific binding) of the cell suspension. For total binding, DMSO/H_2O (2:8 v/v) (50 µL) and DMSO/H_2O (1:1 v/v) (50 µL), containing **20** (100 nM), **23** (500 nM) or **28** (350 nM), were added. To determine unspecific binding, DMSO/H_2O (2:8 v/v) (25 µL), containing **31** (50, 250 and 175 µM, respectively), and DMSO/H_2O (1:1 v/v) (25 µL), containing **20** (100 nM), **23** (500 nM) or **28** (350 nM), were added to the cell suspension followed by incubation under gentle shaking in the dark. After different periods of time (1-300 min), aliquots (200 µL) were taken and subjected to measurement. In the case of dissociation experiments, cells were preincubated with **20** (3 nM), **23** (15 nM) or **28** (10 nM) for 180 min (**20**), 120 min (**23**) or 110 min (**28**). Vessels and sample volumes were the same as for association experiments. Unspecific binding was determined in the presence of **31** at final concentrations of 1.5, 7.5 and 5 µM, respectively. After preincubation with the fluorescent ligand under gentle shaking in the dark, the dissociation was started by the addition of **31** (100-fold concentrated in DMSO/water (2:8 v/v)) to reach final concentrations of **31** of 3, 15 and 10 µM, respectively. After different periods of time (2-540 min), aliquots (200 µL) were taken and subjected to measurement. Dissociation experiments with **23** in the presence of the allosteric M_2R ligands **32**, **33** or **34**, were performed as dissociation experiments in the absence of **32-34**, but 1 min before the start of the dissociation by the addition of **31**, compound **32**, **33** or **34** (10 µM in DMSO**)** was added to reach a final concentration of 100 µM.

High-content imaging binding experiments. One day prior to the experiment, CHO-hM_2R or CHO-hM_1R cells were seeded at 35,000-40,000 cells per well into the central 60 wells of a black clear bottomed 96-well plate (Greiner 655090). On the day of the experiment the medium

was removed by suction, the cells were washed with HBSS[75] containing 0.1 % BSA (in the following referred to as HBSS-BSA) (50 µL), and covered with HBSS-BSA (80 µL) containing the permeable nuclear Hoechst dye H33342 (2 µg/mL). To determine total binding (saturation and competition binding experiments), HBSS-BSA (10 µL) and HBSS-BSA (10 µL) containing the fluorescent ligand (10-fold concentrated) were added. For the determination of unspecific binding and to study the effect of a compound of interest on M_2R binding of the fluorescent ligand (competition binding assay), HBSS-BSA (10 µL) containing **31** or the 'competitor' (10-fold concentrated) and HBSS-BSA (10 µL) containing the fluorescent ligand (10-fold concentrated) were added. Samples were incubated at rt in the dark for 60 min. After incubation, images were directly acquired with the IX Ultra confocal plate reader (Molecular Devices, Sunnyvale CA) (to obtain "non-washing" saturation binding curves) or the cells were washed with HBSS-BSA (50 µL) and covered with HBSS-BSA (50 µL) followed by immediate acquisition of the images using the IX Ultra confocal plate reader. The washing procedure was performed within < 3 min. The excitation laser lines of the Ultra plate reader were 405 nm (H33342) and 635 nm (Cy5). Two sites/well were measured throughout. The following final concentrations of **18**, **20**, **23** and **28** were applied for saturation binding studies: 0.1-70 nM (**18** and **20**, M_2R), 0.4-400 nM (**23**, M_1R), 0.4-200 nM (**23**, M_2R), and 0.2-100 nM (**28**, M_1R and M_2R). For competition binding experiments at CHO-hM_2R cells, **18**, **20**, **23** and **28** were applied at final concentrations of 10 nM. For the determination of unspecific binding, **31** was used at 500-fold (saturation binding) or 100-fold (competition binding) excess to the fluorescent ligand. Saturation binding experiments were performed in triplicate and competition binding assays were performed in duplicate. M_2R saturation binding experiments with **20**, **23** and **28** in the presence of **32** (Schild analysis) were performed as described above with the following modification: the cells were covered with 70 µL of HBSS-BSA instead of 80 µL to compensate the extra addition of HBSS-BSA (10 µL) containing **32** (10-fold concentrated). The washing step prior to the measurement was performed.

Confocal Microscopy. For the investigation of binding of **20**, **23** and **28** to CHO-hM_2R cells by confocal microscopy, a previously described protocol for studying binding of fluorescently labeled neurotensin receptor ligands to CHO-hNTS_1R cells, was used.[27] The final fluorescent ligand concentration was 30 nM. Unspecific binding was determined in the presence of **31** (10 μM). Images were acquired after an incubation period of 5-45 min with a Zeiss LSM 710 confocal laser scanning microscope (Zeiss, Jena, Germany). The objective was 63× magnification with oil (1.4 NA). The excitation laser lines were 405 nm and 633 nm, filter settings were 410-514 nm (H33342 channel) and 638-759 nm (Cy5 channel), and the pinhole setting was 1.0 airy unit for the Cy5 channel.

Molecular dynamics simulation. For induced-fit docking, ligand (**23**, **28**) geometries were energetically optimized using the LigPrep module (Schrödinger LLC). Tertiary amine groups and imidazole moieties in **23** and **28** were protonated, and sulfonic acid groups were deprotonated resulting in net charges of +1 and +3, respectively. Induced-fit docking (Schrödinger LLC) of **23** was performed using the output coordinates of the previously described docking of **6** at the hM_2R.[38] For initial docking, Y104$^{3.33}$, Y403$^{6.51}$, and Y426$^{7.39}$ were mutated to alanine, and **23** was docked within a box of 46 × 46 × 46 Å^3 around the binding pose of **6**. For redocking, the extended precision protocol was used. Induced-fit docking of **28** was performed using the output coordinates of the docking of **23**. Initial docking was performed by analogy to that of **23**, but core restraints were applied to the N^5-((piperidin-1-yl)ethanoyl)dibenzodiazepinone partial structure with a maximum RMSD of 5 Å based on the identical partial structure of **23**. For redocking, the mutations of Y104$^{3.33}$, Y403$^{6.51}$, and Y426$^{7.39}$ to alanine as well as the core restraints were maintained, and, after redocking, a second prime refinement stage was applied (including a reversion of the alanine mutations). The binding poses, corresponding to the lowest XP GScore, were selected as initial coordinates for MD

simulations. The respective ligand-receptor complexes were aligned to the hM_2R entry (PDB ID: 3UON) in the orientations of proteins in membranes (OPM) database[76] using the protein structure alignment tool (Schrödinger LLC). The ligand-receptor complexes were inserted into a hydrated palmitoyloleoylphosphatidylcholine (POPC) bilayer (comprising 160 POPC molecules) as described for **6**.[38] The systems contained about 62,000 (**23**) and 65,000 (**28**) atoms and the initial box size was approximately 81 × 81 × 102 $Å^3$ and 81 × 81 × 106 $Å^3$, respectively. The parameters (geometry, partial charges) of the protein structure, compounds **23** and **28**, lipids, inorganic ions, and water were assigned as reported.[38] MD simulations were executed on Nvidia GTX 1080Ti GPUs (approximately 11.5 TFlops) using the CUDA version of PMEMD,[77,78] implemented in AMBER18 (AMBER 2018, University of California, San Francisco, CA). After minimization, the systems were heated from 0 to 100 °K in the NVT ensemble during 20 ps and from 100 to 310 °K in the NPT ensemble during 100 ps, applying harmonic restraints of 5 kcal mol^{-1} $Å^{-1}$ to non-hydrogen atoms of protein, lipids and ligand. The temperature and pressure coupling parameters used for the equilibration at 310 °K (NPT ensemble) were the same as described for MD simulations of the hM_2R bound to **6**.[38] During the 10 ns equilibration period, harmonic restraints on receptor non-hydrogen atoms were reduced stepwise (0.5 kcal mol^{-1} $Å^{-1}$ every 0.5 ns) to 0.5 kcal mol^{-1} $Å^{-1}$ within 5 ns. Harmonic restraints on ligand non-hydrogen atoms were reduced stepwise (0.5 kcal mol^{-1} $Å^{-1}$ every 0.5 ns) to 2.5 kcal mol^{-1} $Å^{-1}$ within 3 ns. After 5 and 3 ns, respectively, harmonic restraints on receptor and ligand non-hydrogen atoms were removed, i.e. the residual equilibration period (5 ns) was run without restraints. The interaction cutoff was set to 9.0 Å. Long-range electrostatics were computed using the particle mesh Ewald (PME) method.[79] To enable a frame step size of 4 fs, bonds involving hydrogen atoms were constrained using SHAKE[80] and hydrogen mass repartitioning (HMR)[81] was applied. The final frame of the equilibration period was used as input for the simulations over 5.25 μs. After the equilibration period of 10 ns, the Berendsen Barostat was replaced by the Monte Carlo Barostat algorithm.[82] Cluster and H-bond analyses

were performed as described,[38] but data were collected every 500 ps using every tenth frame (5 ns step size). The first 250 ns of the simulations were omitted. Figures showing molecular structures (Figure 9A-D) were generated with PyMOL Molecular Graphics system, version 1.8.2.1 (Schrödinger LLC).

Data processing. Retention (capacity) factors were calculated from retention times (t_R) according to $k = (t_R - t_0)/t_0$ (t_0 = dead time). Data from the IP1 accumulation assay were processed as described previously, but pIC_{50} values were not converted to pK_b values.[38] Raw data from flow cytometric experiments were processed with the aid of the FlowJo software (FlowJo LLC, Ashland, OR) to obtain geometrical mean values of FL-4 (FACSCalibur), or using the FACSDiva Software (Becton Dickinson) to obtain arithmetic mean values of the APC-A channel (FACSCanto II). Fluorescence arbitrary values from high-content imaging fluorescence images were obtained using a previously described procedure.[13,27] Specific binding data from saturation binding experiments (flow cytometry, high-content imaging), obtained by subtracting unspecific binding data from total binding data, were plotted against the fluorescent ligand concentration and analyzed by a two-parameter equation describing hyperbolic binding (one site-specific binding, GraphPad Prism 5, GraphPad Software, San Diego, CA) to obtain K_d and B_{max} values. Unspecific binding data were fitted by linear regression. Additionally, specific binding data were plotted against log(fluorescent ligand concentration) and analyzed by a four-parameter logistic fit (log(agonist) vs. response, applied constraints: bottom = 0%, top = B_{max} of the aforementioned two-parameter hyperbolic fit; GraphPad Prism) to obtain pK_d values. In case of saturation binding experiments in the presence of compound **32**, specific binding data were analyzed by a two-parameter equation describing hyperbolic binding (one site-specific binding, GraphPad Prism) to obtain K_d and B_{max} values. Additionally, specific binding data were normalized to the B_{max} value, specific binding (%) was plotted against log(concentration **20**, **23** or **28**) followed by analysis using a four-parameter

logistic fit (log(agonist) vs. response, applied constraints: bottom = 0%, top = 100%, slope = 1; GraphPad Prism). Data for the 'Schild' plot were obtained from the rightward shift (ΔpK_d) of the saturation isotherm and transformation into log(r−1) (where $r = 10^{\Delta pKd}$). Log(r−1) was plotted against log(concentration of **32**) and the data were analyzed by linear regression to obtain the slope and the 'pA_2' value (intercept with the X axis). Specific binding data from association experiments with **20**, **23** and **28** (flow cytometry) were analyzed by a two-parameter equation describing an exponential rise to a maximum (one-phase association) (SigmaPlot 11.0, Systat Software, Chicago, IL) to obtain the observed association rate constant k_{obs} and the maximum of specifically bound fluorescent ligand (B_{eq}), which was used to calculate specifically bound fluorescent ligand (B_t) in %. Data from dissociation experiments (flow cytometry) (% specifically bound fluorescent ligand (B_t) plotted over time) were analyzed by a three-parameter equation (incomplete one phase decay, SigmaPlot 11.0). The association rate constants (k_{on}) of **20**, **23** and **28** were calculated from k_{obs}, k_{off} and the concentration of the fluorescent ligand used for the determination of k_{obs} ([fluorescent ligand]) according to the equation: $k_{on} = (k_{obs} - k_{off})/[\text{fluorescent ligand}]$. The kinetically derived dissociation constants K_d(kin) of **20**, **23** and **28** were calculated according to: $K_d(\text{kin}) = k_{off}/k_{on}$. Total binding data from competition binding experiments (radiochemical assays, flow cytometry, high-content imaging) were plotted against log(concentration competitor) and analyzed by a four-parameter logistic equation (log(inhibitor) vs response - variable slope, GraphPad Prism) followed by normalization (100% = "top" of the four-parameter logistic fit, 0% = unspecifically bound radioligand or fluorescent ligand) and analysis of the normalized data by a four-parameter logistic equation to obtain pIC_{50} values. The latter were converted to pK_i values according to the Cheng-Prusoff equation[83] (logarithmic form). Statistical significance (curve slopes) was assessed by a one-sample, two-tailed t-test. Propagated errors were calculated according to the general equation (1) (maximum error propagation).

$$\Delta z = \left|\frac{\partial f}{\partial x_1}\right|\Delta x_1 + \left|\frac{\partial f}{\partial x_2}\right|\Delta x_2 + \ldots \quad (1)$$

f: function of x_1, x_2, etc. ($f(x_1, x_2, \ldots) = z$); Δx_1, Δx_2: error (in this work represented by the SEM) of x_1 and x_2; Δz: (propagated) error of z

Corresponding Author Information

*E-mail addresses: max.keller@ur.de (M.K.), nicholas.holliday@nottingham.ac.uk (N.D.H.) Tel.: (+49)941 9433329 (M.K.), (+44)115 8230084 (N.D.H.)

Fax: (+49)941 9434820 (M.K.)

Present/Current author addresses

[$]Moffitt Cancer Center, 12902 Magnolia Drive, Tampa, Florida 33612, United States

[€]Ramboll Environment & Health GmbH, Werinherstraße 79, 81541 Munich, Germany

[¥]Leibniz Supercomputing Centre of the Bavarian Academy of Sciences and Humanities, Boltzmannstraße 1, 85748 Garching, Germany

[⊥]Sanofi, R&D China, 3/F, No. 108, Jian Guo Avenue, Chaoyang District, Beijing, 100022, China

[§]Chengdu Kanghong Pharmaceutical Group Co. Ltd., No. 36, Shuxi Road, Jinniu District, Chengdu, 610036, China

Author Contributions

[#]These authors contributed equally. X.S., A.P., M.K., M.C. and J.W. synthesized and analytically characterized the florescent ligands. X.S., A.P., M.K. and C.G.G.

performed radiochemical and flow cytometric binding experiments and analyzed the data. X.S. and A.P. performed high-content imaging binding studies. H.H. and P.G. performed IP1 accumulation assays and analyzed the data. J.C. and N.D.H. performed confocal microscopy studies. D.W. performed MD simulations and processed the data. M.K. initiated and planned the project. M.K., N.D.H. and G.B. supervised the research. X.S., A.P., M.K., N.D.H., D.W. and G.B. wrote the manuscript. All authors have given approval to the final version of the manuscript.

Notes

The authors declare no competing financial interest.

Acknowledgement

The authors thank Brigitte Wenzl, Elvira Schreiber, Maria Beer-Krön, Dita Fritsch, and Susanne Bollwein for excellent technical assistance, Armin Buschauer for providing laboratory equipment and for helpful suggestions, as well as Seema Rajani and the School of Life Sciences imaging (SLIM) team (University of Nottingham) for their support in microscopy and analysis. Furthermore, the authors thank the Leibnitz Supercomputing Centre (LRZ) in Munich for providing software (Schrödinger Suite) and computing resources. This work was funded by the Graduate Training Program (Graduiertenkolleg) GRK1910 of the Deutsche Forschungsgemeinschaft (DFG) and by the China Scholarship Council (CSC).

Abbreviations Used

B_0, specifically bound (fluorescent) ligand after the pre-incubation (before the start of the dissociation) of a dissociation experiment; B_{eq}, estimated maximum of specifically bound (fluorescent) ligand of an association experiment; B_t, specifically bound (fluorescent) ligand at time "t" of an association or a dissociation experiment; CCh, carbachol; MeCN, acetonitrile; CHO-cells, Chinese hamster ovary cells; DIPEA, diisopropylethylamine; GPCR, G-protein coupled receptor; HBSS, Hank's balanced salt solution; IP1, inositol monophosphate; *k*, retention (or capacity) factor (HPLC); K_d, dissociation constant obtained from a saturation binding experiment; k_{obs}, observed association rate constant; k_{off}, dissociation rate constant; k_{on}, association rate constant; MR, muscarinic receptor; NMS, N-methylscopolamine; PBS, phosphate buffered saline; pK_b, negative logarithm of the dissociation constant K_b (in M) of an antagonist determined by inhibition of the response elicited by an agonist (functional assay); pK_d, negative logarithm of the K_d in M; pK_i, negative logarithm of the dissociation constant K_i (in M) obtained from a competition binding experiment; RMSD, root mean square deviation; TFA, trifluoroacetic acid; t_R, retention time.

ASSOCIATED CONTENT

Supporting Information Available: Figures S1-S11; Table S1; RP-HPLC chromatograms of compounds **10**, **12**, **14**, **16-18**, **20**, **22**, **23**, **27**, **28** and **30**; ^{1}H-NMR spectra of compounds **10**, **12**, **14**, **17**, **18**, **20**, **22**, **23**, **27**, **28** and **30**; molecular formula strings (CSV).

References

(1) Stoddart, L. A.; Kilpatrick, L. E.; Briddon, S. J.; Hill, S. J. Probing the pharmacology of G protein-coupled receptors with fluorescent ligands. *Neuropharmacology* **2015**, *98*, 48-57.

(2) Stoddart, L. A.; White, C. W.; Nguyen, K.; Hill, S. J.; Pfleger, K. D. G. Fluorescence- and bioluminescence-based approaches to study GPCR ligand binding. *Br. J. Pharmacol.* **2016**, *173*, 3028-3037.

(3) Stoddart, L. A.; Kilpatrick, L. E.; Hill, S. J. NanoBRET approaches to study ligand binding to GPCRs and RTKs. *Trends Pharmacol. Sci.* **2018**, *39*, 136-147.

(4) Rinken, A.; Veiksina, S.; Kopanchuk, S. Dynamics of ligand binding to GPCR: residence time of melanocortins and its modulation. *Pharmacol. Res.* **2016**, *113*, 747-753.

(5) Rinken, A.; Lavogina, D.; Kopanchuk, S. Assays with detection of fluorescence anisotropy: challenges and possibilities for characterizing ligand binding to GPCRs. *Trends Pharmacol. Sci.* **2018**, *39*, 187-199.

(6) Middleton, R. J.; Kellam, B. Fluorophore-tagged GPCR ligands. *Curr. Opin. Chem. Biol.* **2005**, *9*, 517-525.

(7) Kuder, K.; Kiec-Kononowicz, K. Fluorescent GPCR ligands as new tools in pharmacology. *Curr. Med. Chem.* **2008**, *15*, 2132-2143.

(8) Kuder, K. J.; Kiec-Kononowicz, K. Fluorescent GPCR ligands as new tools in pharmacology-update, years 2008- early 2014. *Curr. Med. Chem.* **2014**, *21*, 3962-3975.

(9) Dumont, Y.; Gaudreau, P.; Mazzuferi, M.; Langlois, D.; Chabot, J. G.; Fournier, A.; Simonato, M.; Quirion, R. BODIPY-conjugated neuropeptide Y ligands: new fluorescent tools to tag Y_1, Y_2, Y_4 and Y_5 receptor subtypes. *Br. J. Pharmacol.* **2005**, *146*, 1069-1081.

(10) Ziemek, R.; Brennauer, A.; Schneider, E.; Cabrele, C.; Beck-Sickinger, A. G.; Bernhardt, G.; Buschauer, A. Fluorescence- and luminescence-based methods for the determination of affinity and activity of neuropeptide Y_2 receptor ligands. *Eur. J. Pharmacol.* **2006**, *551*, 10-18.

(11) Schneider, E.; Keller, M.; Brennauer, A.; Hoefelschweiger, B. K.; Gross, D.; Wolfbeis, O. S.; Bernhardt, G.; Buschauer, A. Synthesis and characterization of the first fluorescent nonpeptide NPY Y_1 receptor antagonist. *ChemBioChem* **2007**, *8*, 1981-1988.

(12) Keller, M.; Erdmann, D.; Pop, N.; Pluym, N.; Teng, S.; Bernhardt, G.; Buschauer, A. Red-fluorescent argininamide-type NPY Y_1 receptor antagonists as pharmacological tools. *Bioorg. Med. Chem.* **2011**, *19*, 2859-2878.

(13) Liu, M.; Richardson, R. R.; Mountford, S. J.; Zhang, L.; Tempone, M. H.; Herzog, H.; Holliday, N. D.; Thompson, P. E. Identification of a cyanine-dye labeled peptidic ligand for Y_1R and Y_4R, based upon the neuropeptide Y C-terminal analogue, BVD-15. *Bioconjug. Chem.* **2016**, *27*, 2166-2175.

(14) Dukorn, S.; Littmann, T.; Keller, M.; Kuhn, K.; Cabrele, C.; Baumeister, P.; Bernhardt, G.; Buschauer, A. Fluorescence- and radiolabeling of [Lys^4,$Nle^{17,30}$]hPP yields molecular tools for the NPY Y_4 receptor. *Bioconjugate Chem.* **2017**, *28*, 1291-1304.

(15) Li, L.; Kracht, J.; Peng, S.; Bernhardt, G.; Buschauer, A. Synthesis and pharmacological activity of fluorescent histamine H_1 receptor antagonists related to mepyramine. *Bioorg. Med. Chem. Lett.* **2003**, *13*, 1245-1248.

(16) Li, L.; Kracht, J.; Peng, S.; Bernhardt, G.; Elz, S.; Buschauer, A. Synthesis and pharmacological activity of fluorescent histamine H_2 receptor antagonists related to potentidine. *Bioorg. Med. Chem. Lett.* **2003**, *13*, 1717-1720.

(17) Malan, S. F.; van Marle, A.; Menge, W. M.; Zuliani, V.; Hoffman, M.; Timmerman, H.; Leurs, R. Fluorescent ligands for the histamine H_2 receptor: synthesis and preliminary characterization. *Bioorg. Med. Chem.* **2004**, *12*, 6495-6503.

(18) Amon, M.; Ligneau, X.; Schwartz, J. C.; Stark, H. Fluorescent non-imidazole histamine H_3 receptor ligands with nanomolar affinities. *Bioorg. Med. Chem. Lett.* **2006**, *16*, 1938-1940.

(19) Xie, S. X.; Petrache, G.; Schneider, E.; Ye, Q. Z.; Bernhardt, G.; Seifert, R.; Buschauer, A. Synthesis and pharmacological characterization of novel fluorescent histamine H_2-receptor ligands derived from aminopotentidine. *Bioorg. Med. Chem. Lett.* **2006**, *16*, 3886-3890.

(20) Arttamangkul, S.; Alvarez-Maubecin, V.; Thomas, G.; Williams, J. T.; Grandy, D. K. Binding and internalization of fluorescent opioid peptide conjugates in living cells. *Mol. Pharmacol.* **2000**, *58*, 1570-1580.

(21) Balboni, G.; Salvadori, S.; Dal Piaz, A.; Bortolotti, F.; Argazzi, R.; Negri, L.; Lattanzi, R.; Bryant, S. D.; Jinsmaa, Y.; Lazarus, L. H. Highly selective fluorescent analogue of the potent delta-opioid receptor antagonist Dmt-Tic. *J. Med. Chem.* **2004**, *47*, 6541-6546.

(22) Houghten, R. A.; Dooley, C. T.; Appel, J. R. De novo identification of highly active fluorescent kappa opioid ligands from a rhodamine labeled tetrapeptide positional scanning library. *Bioorg. Med. Chem. Lett.* **2004**, *14*, 1947-1951.

(23) Leopoldo, M.; Lacivita, E.; Passafiume, E.; Contino, M.; Colabufo, N. A.; Berardi, F.; Perrone, R. 4-[omega-[4-arylpiperazin-1-yl]alkoxy]phenyl)imidazo[1,2-a]pyridine derivatives: fluorescent high-affinity dopamine D_3 receptor ligands as potential probes for receptor visualization. *J. Med. Chem.* **2007**, *50*, 5043-5047.

(24) Tabor, A.; Weisenburger, S.; Banerjee, A.; Purkayastha, N.; Kaindl, J. M.; Huebner, H.; Wei, L.; Groemer, T. W.; Kornhuber, J.; Tschammer, N.; Birdsall, N. J. M.; Mashanov, G. I.; Sandoghdar, V.; Gmeiner, P. Visualization and ligand-induced modulation of dopamine receptor dimerization at the single molecule level. *Sci. Rep.* **2016**, *6*, 33233.

(25) Keller, M.; Kuhn, K. K.; Einsiedel, J.; Hubner, H.; Biselli, S.; Mollereau, C.; Wifling, D.; Svobodova, J.; Bernhardt, G.; Cabrele, C.; Vanderheyden, P. M.; Gmeiner, P.; Buschauer, A. Mimicking of arginine by functionalized N(omega)-carbamoylated arginine as a new broadly applicable approach to labeled bioactive peptides: high affinity angiotensin, neuropeptide Y, neuropeptide FF, and neurotensin receptor ligands as examples. *J. Med. Chem.* **2016**, *59*, 1925-1945.

(26) Faure, M. P.; Gaudreau, P.; Shaw, I.; Cashman, N. R.; Beaudet, A. Synthesis of a biologically active fluorescent probe for labeling neurotensin receptors. *J. Histochem. Cytochem.* **1994**, *42*, 755-763.

(27) Keller, M.; Mahuroof, S. A.; Hong Yee, V.; Carpenter, J.; Schindler, L.; Littmann, T.; Pegoli, A.; Hubner, H.; Bernhardt, G.; Gmeiner, P.; Holliday, N. D. Fluorescence labeling of neurotensin(8-13) via arginine residues gives molecular tools with high receptor affinity. *ACS Med. Chem. Lett.* **2020**, *11*, 16-22.

(28) Spinnler, K.; von Kruchten, L.; Konieczny, A.; Schindler, L.; Bernhardt, G.; Keller, M. An alkyne-functionalized arginine for solid-phase synthesis enabling "bioorthogonal" peptide conjugation. *ACS Med. Chem. Lett.* **2020**, *11*, 334-339.

(29) Kozma, E.; Jayasekara, P. S.; Squarcialupi, L.; Paoletta, S.; Moro, S.; Federico, S.; Spalluto, G.; Jacobson, K. A. Fluorescent ligands for adenosine receptors. *Bioorg. Med. Chem. Lett.* **2013**, *23*, 26-36.

(30) Tahtaoui, C.; Parrot, I.; Klotz, P.; Guillier, F.; Galzi, J. L.; Hibert, M.; Ilien, B. Fluorescent pirenzepine derivatives as potential bitopic ligands of the human M_1 muscarinic receptor. *J. Med. Chem.* **2004**, *47*, 4300-4315.

(31) Daval, S. B.; Kellenberger, E.; Bonnet, D.; Utard, V.; Galzi, J.-L.; Ilien, B. Exploration of the orthosteric/allosteric interface in human M_1 muscarinic receptors by bitopic fluorescent ligands. *Mol. Pharmacol.* **2013**, *84*, 71-85.

(32) Harris, A.; Cox, S.; Burns, D.; Norey, C. Miniaturization of fluorescence polarization receptor-binding assays using CyDye-labeled ligands. *J. Biomol. Screening* **2003**, *8*, 410-420.

(33) Jones, L. H.; Randall, A.; Napier, C.; Trevethick, M.; Sreckovic, S.; Watson, J. Design and synthesis of a fluorescent muscarinic antagonist. *Bioorg. Med. Chem. Lett.* **2008**, *18*, 825-827.

(34) Hern, J. A.; Baig, A. H.; Mashanov, G. I.; Birdsall, B.; Corrie, J. E. T.; Lazareno, S.; Molloy, J. E.; Birdsall, N. J. M. Formation and dissociation of M_1 muscarinic receptor dimers seen by total internal reflection fluorescence imaging of single molecules. *Proc. Natl. Acad. Sci. U. S. A.* **2010**, *107*, 2693-2698.

(35) Daval, S. B.; Valant, C.; Bonnet, D.; Kellenberger, E.; Hibert, M.; Galzi, J. L.; Ilien, B. Fluorescent derivatives of AC-42 to probe bitopic orthosteric/allosteric binding mechanisms on muscarinic M_1 receptors. *J. Med. Chem.* **2012**, *55*, 2125-2143.

(36) Nenasheva, T. A.; Neary, M.; Mashanov, G. I.; Birdsall, N. J.; Breckenridge, R. A.; Molloy, J. E. Abundance, distribution, mobility and oligomeric state of M(2) muscarinic acetylcholine receptors in live cardiac muscle. *J. Mol. Cell. Cardiol.* **2013**, *57*, 129-136.

(37) Mazzone, S. B.; Mori, N.; Burman, M.; Palovich, M.; Belmonte, K. E.; Canning, B. J. Fluorescent styryl dyes FM1-43 and FM2-10 are muscarinic receptor antagonists: intravital visualization of receptor occupancy. *J. Physiol.* **2006**, *575*, 23-35.

(38) Pegoli, A.; She, X.; Wifling, D.; Hübner, H.; Bernhardt, G.; Gmeiner, P.; Keller, M. Radiolabeled dibenzodiazepinone-type antagonists give evidence of dualsteric binding at the M_2 muscarinic acetylcholine receptor. *J. Med. Chem.* **2017**, *60*, 3314-3334.

(39) She, X.; Pegoli, A.; Mayr, J.; Huebner, H.; Bernhardt, G.; Gmeiner, P.; Keller, M. Heterodimerization of dibenzodiazepinone-type muscarinic acetylcholine receptor ligands leads to increased M_2R affinity and selectivity. *ACS Omega* **2017**, *2*, 6741-6754.

(40) Gitler, M. S.; Reba, R. C.; Cohen, V. I.; Rzeszotarski, W. J.; Baumgold, J. A novel m2-selective muscarinic antagonist: binding characteristics and autoradiographic distribution in rat brain. *Brain Res.* **1992**, *582*, 253-260.

(41) She, X. Synthesis and pharmacological characterization of dibenzodiazepinone-type heterodimeric and fluorescently labeled muscarinic receptor ligands. Doctoral thesis. University of Regensburg, Regensburg, Germany, 2017, *https://epub.uni-regensburg.de/35508/*.

(42) Keller, M.; Tränkle, C.; She, X.; Pegoli, A.; Bernhardt, G.; Buschauer, A.; Read, R. W. M_2 Subtype preferring dibenzodiazepinone-type muscarinic receptor ligands: effect of chemical homo-dimerization on orthosteric (and allosteric?) binding. *Bioorg. Med. Chem.* **2015**, *23*, 3970-3990.

(43) Wetzl, B. K.; Yarmoluk, S. M.; Craig, D. B.; Wolfbeis, O. S. Chameleon labels for staining and quantifying proteins. *Angew. Chem., Int. Ed.* **2004**, *43*, 5400-5402.

(44) Bridges, T. M.; Brady, A. E.; Kennedy, J. P.; Daniels, R. N.; Miller, N. R.; Kim, K.; Breininger, M. L.; Gentry, P. R.; Brogan, J. T.; Jones, C. K. Synthesis and SAR of analogues of the M_1 allosteric agonist TBPB. Part I: exploration of alternative benzyl and privileged structure moieties. *Bioorg. Med. Chem. Lett.* **2008**, *18*, 5439-5442.

(45) Miller, N. R.; Daniels, R. N.; Bridges, T. M.; Brady, A. E.; Conn, P. J.; Lindsley, C. W. Synthesis and SAR of analogs of the M_1 allosteric agonist TBPB. Part II: amides, sulfonamides and ureas—the effect of capping the distal basic piperidine nitrogen. *Bioorg. Med. Chem. Lett.* **2008**, *18*, 5443-5447.

(46) Jones, C. K.; Brady, A. E.; Davis, A. A.; Xiang, Z.; Bubser, M.; Tantawy, M. N.; Kane, A. S.; Bridges, T. M.; Kennedy, J. P.; Bradley, S. R. Novel selective allosteric activator of the M_1 muscarinic acetylcholine receptor regulates amyloid processing and produces antipsychotic-like activity in rats. *J. Neurosci.* **2008**, *28*, 10422-10433.

(47) Keov, P.; Valant, C.; Devine, S. M.; Lane, J. R.; Scammells, P. J.; Sexton, P. M.; Christopoulos, A. Reverse engineering of the selective agonist TBPB unveils both orthosteric and allosteric modes of action at the M_1 muscarinic acetylcholine receptor. *Mol. Pharmacol.* **2013**, *84*, 425-437.

(48) Prinz, H. Hill coefficients, dose-response curves and allosteric mechanisms. *J. Chem. Biol.* **2010**, *3*, 37-44.

(49) Smith, N. J.; Milligan, G. Allostery at G protein-coupled receptor homo- and heteromers: uncharted pharmacological landscapes. *Pharmacol. Rev.* **2010**, *62*, 701-725.

(50) Edelstein, S. J.; Le Novere, N. Cooperativity of allosteric receptors. *J. Mol. Biol.* **2013**, *425*, 1424-1432.

(51) Bindslev, N. Drug-acceptor interactions: modeling theoretical tools to test and evaluate experimental equilibrium effects, open access e-book; 1st ed., Taylor & Francis Group: 2017, https://doi.org/10.4324/9781315159782.

(52) Fish, I.; Stossel, A.; Eitel, K.; Valant, C.; Albold, S.; Huebner, H.; Moller, D.; Clark, M. J.; Sunahara, R. K.; Christopoulos, A.; Shoichet, B. K.; Gmeiner, P. Structure-based design and discovery of new M_2 receptor agonists. *J. Med. Chem.* **2017**, *60*, 9239-9250.

(53) Copeland, R. A. Conformational adaptation in drug-target interactions and residence time. *Future Med. Chem.* **2011**, *3*, 1491-1501.

(54) Vauquelin, G. Simplified models for heterobivalent ligand binding: when are they applicable and which are the factors that affect their target residence time. *Naunyn Schmiedebergs Arch. Pharmacol.* **2013**, *386*, 949-962.

(55) Lüllmann, H.; Ohnesorge, F.; Schauwecker, G.-C.; Wassermann, O. Inhibition of the actions of carbachol and DFP on guinea pig isolated atria by alkane-bis-ammonium compounds. *Eur. J. Pharmacol.* **1969**, *6*, 241-247.

(56) Christopoulos, A.; Lanzafame, A.; Mitchelson, F. Allosteric interactions at muscarinic cholinoceptors. *Clin. Exp. Pharmacol. Physiol.* **1998**, *25*, 185-194.

(57) Holzgrabe, U.; Bender, W.; Botero Cid, H. M.; Staudt, M.; Pick, R.; Pfletschinger, C.; Balatkova, E.; Trankle, C.; Mohr, K. Ligands for the common allosteric site of acetylcholine M_2-receptors: development and application. *Pharm. Acta Helv.* **2000**, *74*, 149-155.

(58) Croy, C. H.; Schober, D. A.; Xiao, H.; Quets, A.; Christopoulos, A.; Felder, C. C. Characterization of the novel positive allosteric modulator, LY2119620, at the muscarinic M_2 and M_4 receptors. *Mol. Pharmacol.* **2014**, *86*, 106-115.

(59) Schober, D. A.; Croy, C. H.; Xiao, H.; Christopoulos, A.; Felder, C. C. Development of a radioligand, [^{3}H]LY2119620, to probe the human M_2 and M_4 muscarinic receptor allosteric binding sites. *Mol. Pharmacol.* **2014**, *86*, 116-123.

(60) Jakubik, J.; Bacakova, L.; El-Fakahany, E. E.; Tucek, S. Positive cooperativity of acetylcholine and other agonists with allosteric ligands on muscarinic acetylcholine receptors. *Mol. Pharmacol.* **1997**, *52*, 172-179.

(61) Tränkle, C.; Weyand, O.; Voigtlander, U.; Mynett, A.; Lazareno, S.; Birdsall, N. J.; Mohr, K. Interactions of orthosteric and allosteric ligands with [^{3}H]dimethyl-W84 at the common allosteric site of muscarinic M_2 receptors. *Mol. Pharmacol.* **2003**, *64*, 180-190.

(62) Christopoulos, A.; Kenakin, T. G protein-coupled receptor allosterism and complexing. *Pharmacol. Rev.* **2002**, *54*, 323-374.

(63) Kenakin, T. *A pharmacology primer: theory, application and methods*; Academic Press: Burlington, MA, 2009.

(64) Hulme, E. C.; Trevethick, M. A. Ligand binding assays at equilibrium: validation and interpretation. *Br. J. Pharmacol.* **2010**, *161*, 1219-1237.

(65) Eberlein, W. G.; Engel, W.; Mihm, G.; Rudolf, K.; Wetzel, B.; Entzeroth, M.; Mayer, N.; Doods, H. N. Structure-activity relationships and pharmacological profile of selective tricyclic antimuscarinics. *Trends Pharmacol. Sci.* **1989**, *Suppl*, 50-54.

(66) Tränkle, C.; Andresen, I.; Lambrecht, G.; Mohr, K. M_2 receptor binding of the selective antagonist AF-DX 384: possible involvement of the common allosteric site. *Mol. Pharmacol.* **1998**, *53*, 304-312.

(67) Bermudez, M.; Rakers, C.; Wolber, G. Structural characteristics of the allosteric binding site represent a key to subtype selective modulators of muscarinic acetylcholine receptors. *Mol. Inform.* **2015**, *34*, 526-530.

(68) Suga, H.; Ehlert, F. J. Effects of asparagine mutagenesis of conserved aspartic acids in helix 2 (D2.50) and 3 (D3.32) of M_1-M_4 muscarinic receptors on the irreversible binding of nitrogen mustard analogs of acetylcholine and McN-A-343. *Biochemistry* **2013**, *52*, 4914-4928.

(69) Thal, D. M.; Sun, B.; Feng, D.; Nawaratne, V.; Leach, K.; Felder, C. C.; Bures, M. G.; Evans, D. A.; Weis, W. I.; Bachhawat, P.; Kobilka, T. S.; Sexton, P. M.; Kobilka, B. K.; Christopoulos, A. Crystal structures of the M_1 and M_4 muscarinic acetylcholine receptors. *Nature* **2016**, *531*, 335-340.

(70) Haga, K.; Kruse, A. C.; Asada, H.; Yurugi-Kobayashi, T.; Shiroishi, M.; Zhang, C.; Weis, W. I.; Okada, T.; Kobilka, B. K.; Haga, T.; Kobayashi, T. Structure of the human M_2 muscarinic acetylcholine receptor bound to an antagonist. *Nature* **2012**, *482*, 547-551.

(71) Pegoli, A.; Wifling, D.; Gruber, C. G.; She, X.; Hubner, H.; Bernhardt, G.; Gmeiner, P.; Keller, M. Conjugation of short peptides to dibenzodiazepinone-type muscarinic acetylcholine receptor ligands determines M_2R selectivity. *J. Med. Chem.* **2019**, *62*, 5358-5369.

(72) Kane, B. E.; Grant, M. K.; El-Fakahany, E. E.; Ferguson, D. M. Synthesis and evaluation of xanomeline analogs - probing the wash-resistant phenomenon at the M_1 muscarinic acetylcholine receptor. *Bioorg. Med. Chem.* **2008**, *16*, 1376-1392.

(73) Hoefelschweiger, B. K. The pyrylium dyes: a new class of biolabels; synthesis, spectroscopy, and application as labels and in general protein assay. Doctoral Thesis. University of Regensburg, Regensburg, Germany, **2005**, http://d-nb.info/975903071/34.

(74) Aldrich, C.; Bertozzi, C.; Georg, G. I.; Kiessling, L.; Lindsley, C.; Liotta, D.; Merz, K. M., Jr.; Schepartz, A.; Wang, S. The ecstasy and agony of assay interference compounds. *J. Med. Chem.* **2017**, *60*, 2165-2168.

(75) Watson, S.-J.; Brown, A. J. H.; Holliday, N. D. Differential signaling by splice variants of the human free fatty acid receptor GPR120. *Mol. Pharmacol.* **2012**, *81*, 631-642.

(76) Lomize, M. A.; Lomize, A. L.; Pogozheva, I. D.; Mosberg, H. I. OPM: orientations of proteins in membranes database. *Bioinformatics* **2006**, *22*, 623-625.

(77) Salomon-Ferrer, R.; Gotz, A. W.; Poole, D.; Le Grand, S.; Walker, R. C. Routine microsecond molecular dynamics simulations with AMBER on GPUs. 2. explicit solvent particle mesh Ewald. *J. Chem. Theory Comput.* **2013**, *9*, 3878-3888.

(78) Le Grand, S.; Götz, A. W.; Walker, R. C. SPFP: Speed without compromise - a mixed precision model for GPU accelerated molecular dynamics simulations. *Comput. Phys. Commun.* **2013**, *184*, 374-380.

(79) Darden, T.; York, D.; Pedersen, L. Particle mesh Ewald: An N·log(N) method for Ewald sums in large systems. *J. Chem. Phys.* **1993**, *98*, 10089-10092.

(80) Ryckaert, J.-P.; Ciccotti, G.; Berendsen, H. J. C. Numerical integration of the cartesian equations of motion of a system with constraints: molecular dynamics of n-alkanes. *J. Comput. Phys.* **1977**, *23*, 327-341.

(81) Hopkins, C. W.; Le Grand, S.; Walker, R. C.; Roitberg, A. E. Long-time-step molecular dynamics through hydrogen mass repartitioning. *J. Chem. Theory Comput.* **2015**, *11*, 1864-1874.

(82) Chow, K.-H.; Ferguson, D. M. Isothermal-isobaric molecular dynamics simulations with Monte Carlo volume sampling. *Comput. Phys. Commun.* **1995**, *91*, 283-289.

(83) Cheng, Y.-C.; Prusoff, W. H. Relation between the inhibition constant K_i and the concentration of inhibitor which causes fifty per cent inhibition (IC_{50}) of an enzymic reaction. *Biochem. Pharmacol.* **1973**, *22*, 3099-3108.

TOC

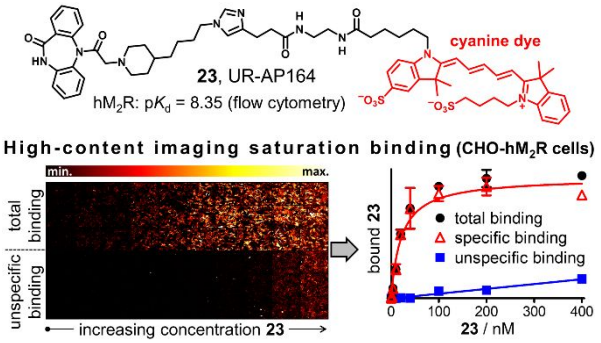
cyanine dye
23, UR-AP164
hM2R: pKd = 8.35 (flow cytometry)
High-content imaging saturation binding (CHO-hM2R cells)
min.
max.
total binding
unspecific binding
increasing concentration 23
bound 23
total binding
specific binding
unspecific binding
0
100
200
300
400
23 / nM

Unable to Convert Image

The dimensions of this image (in pixels) are too large to be converted. For this image to convert, the total number of pixels (height x width) must be less than 40,000,000 (40 megapixels).

Unable to Convert Image

The dimensions of this image (in pixels) are too large to be converted. For this image to convert, the total number of pixels (height x width) must be less than 40,000,000 (40 megapixels).

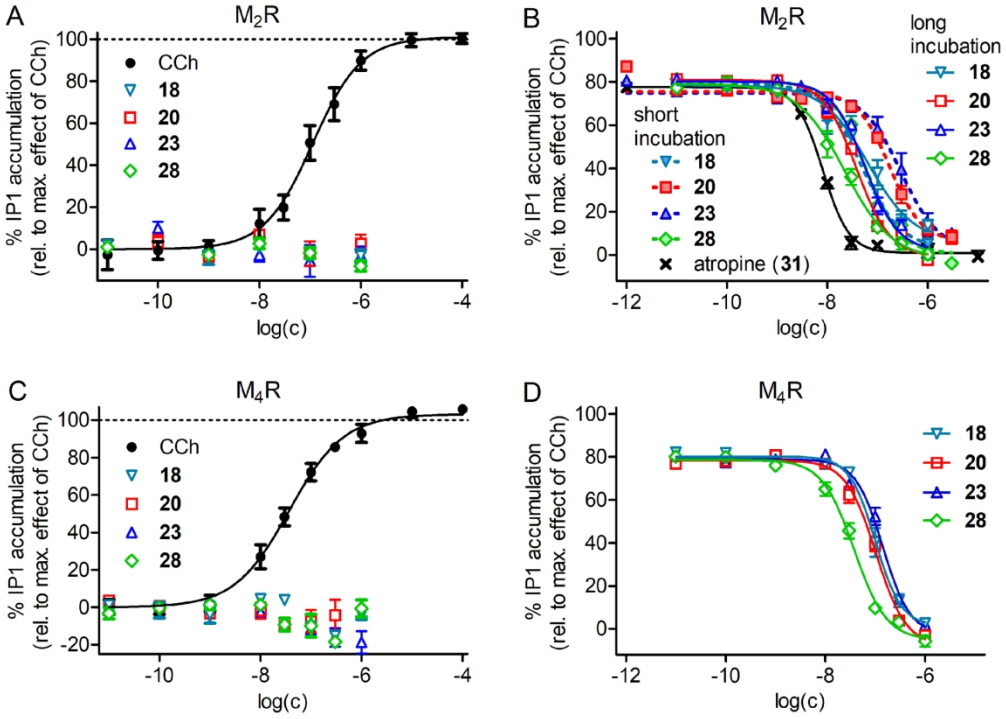

177x126mm (300 x 300 DPI)

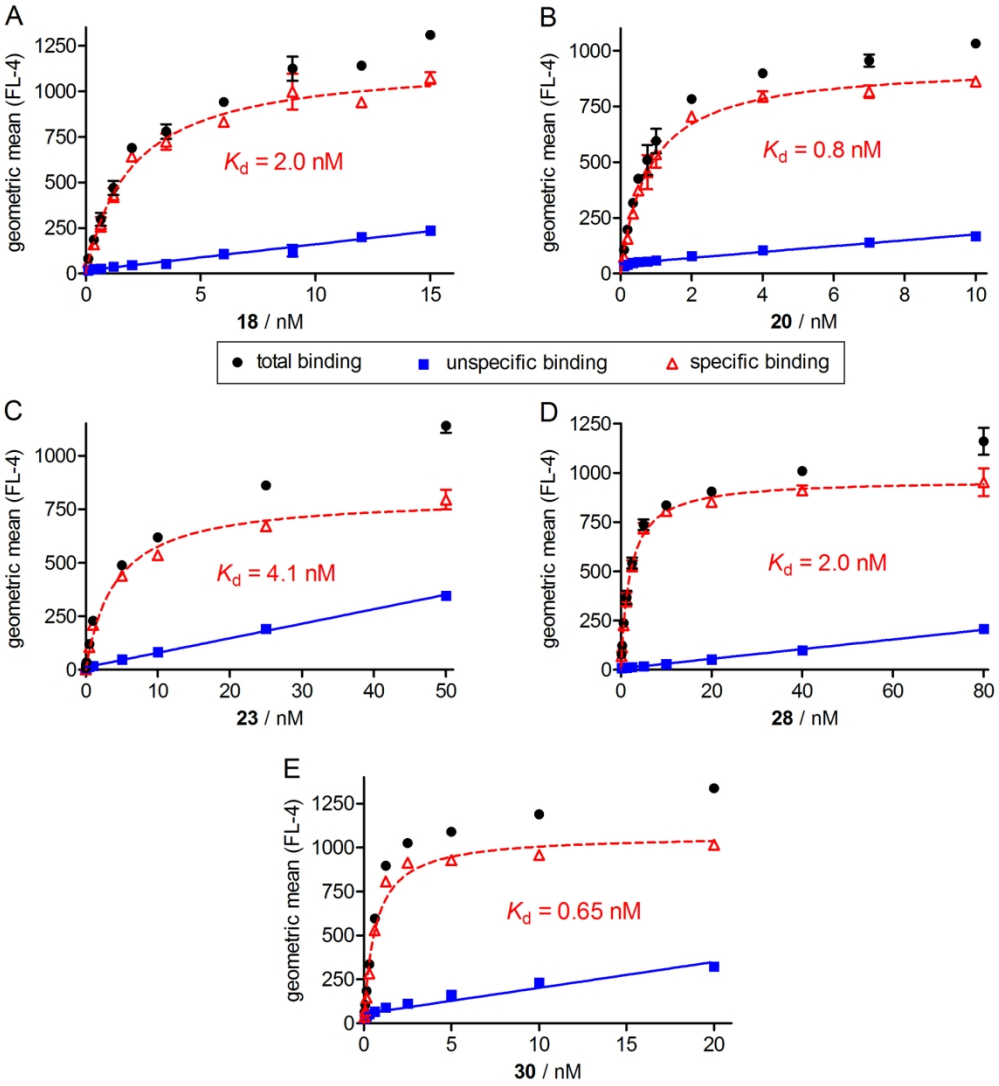

175x188mm (300 x 300 DPI)

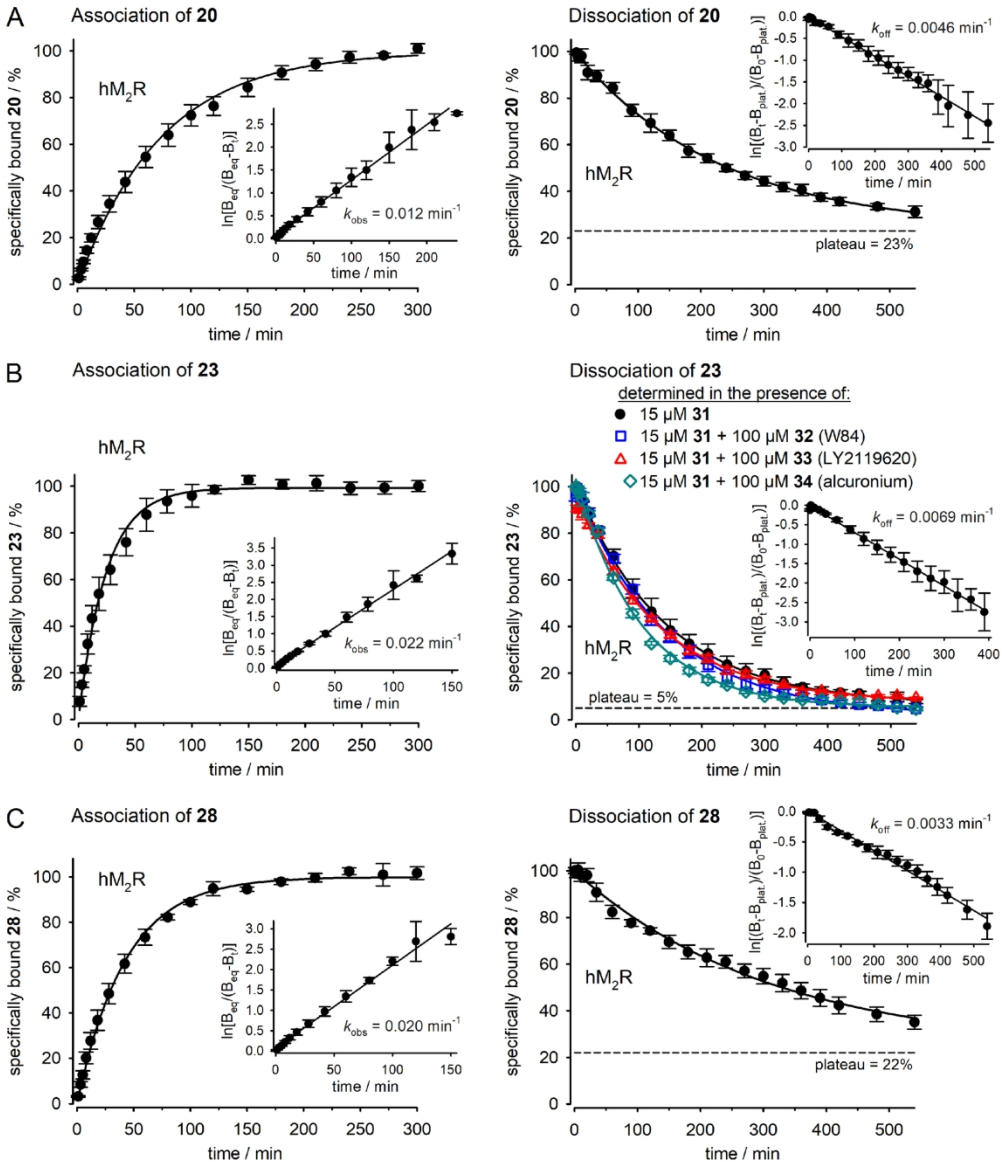

177x207mm (300 x 300 DPI)

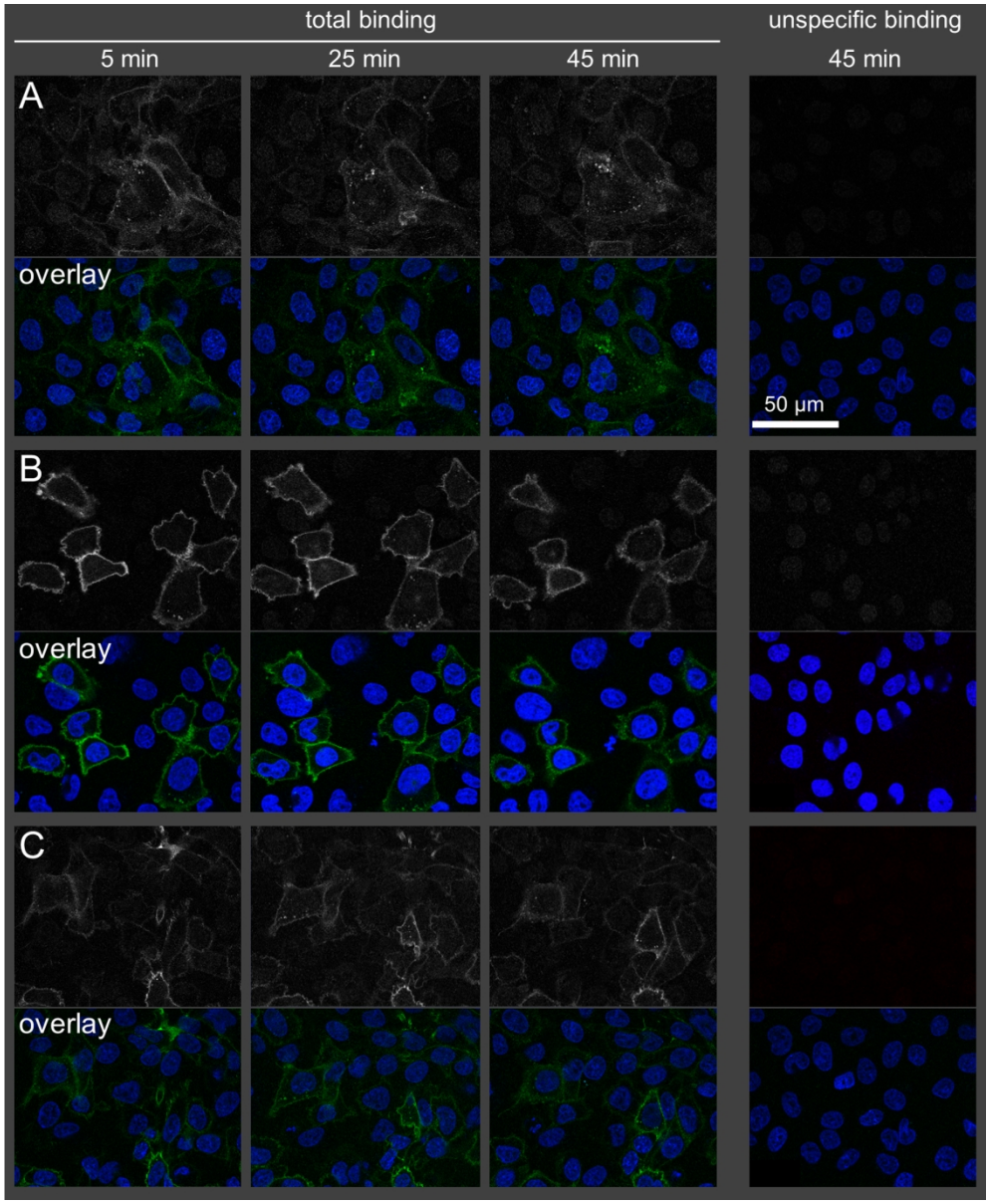

160x194mm (300 x 300 DPI)

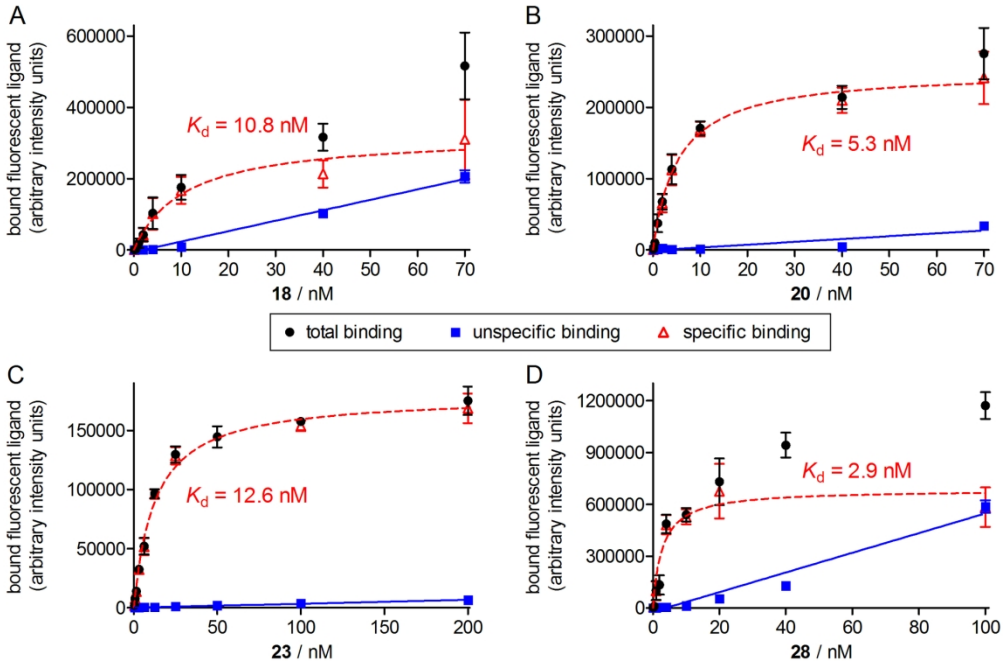

177x116mm (300 x 300 DPI)

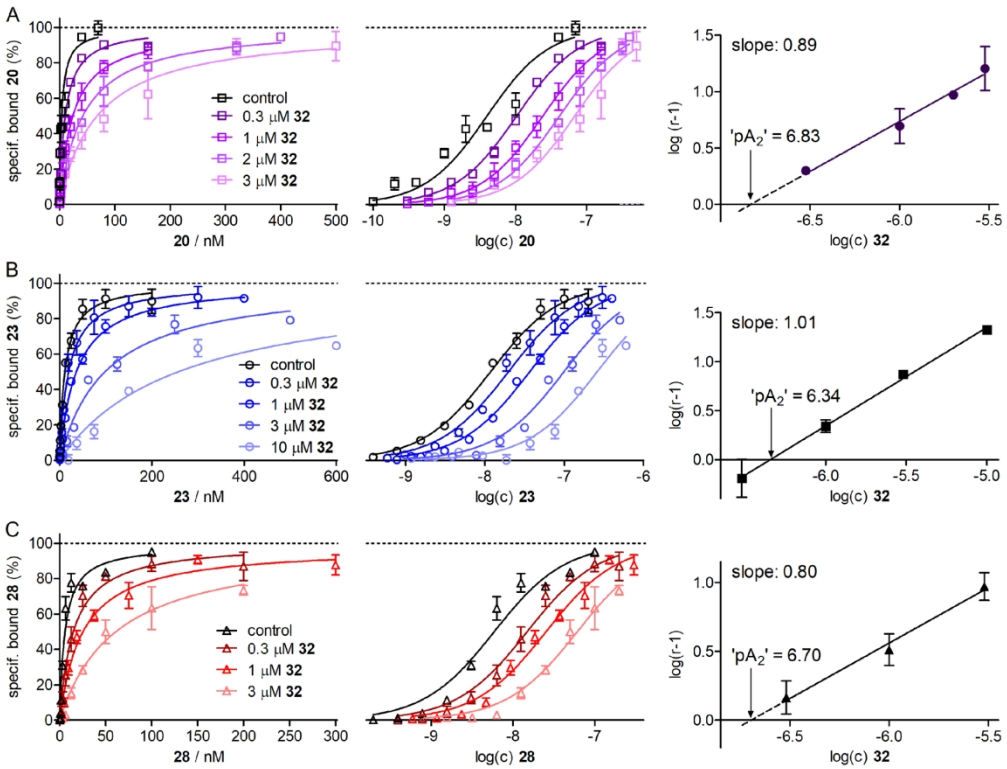

177x135mm (300 x 300 DPI)

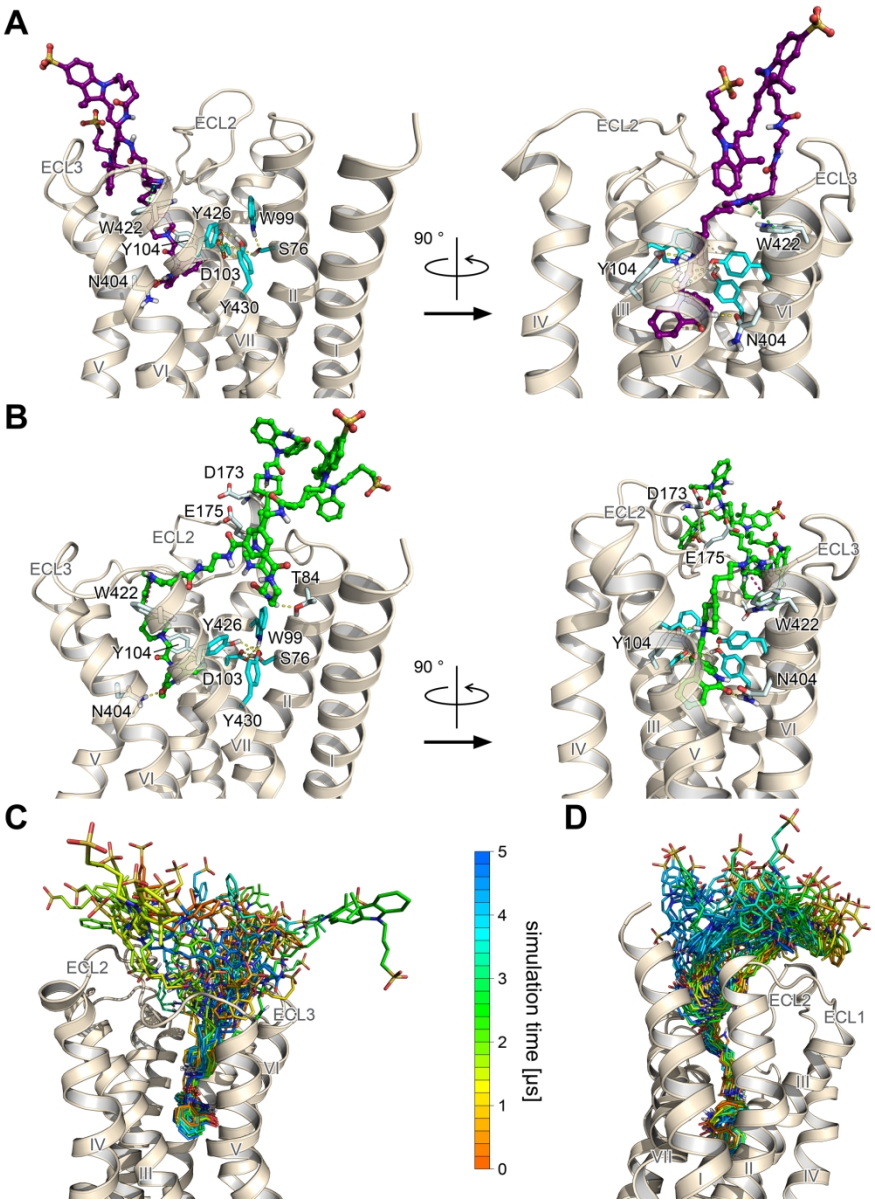

167x229mm (300 x 300 DPI)

Unable to Convert Image

The dimensions of this image (in pixels) are too large to be converted. For this image to convert, the total number of pixels (height x width) must be less than 40,000,000 (40 megapixels).

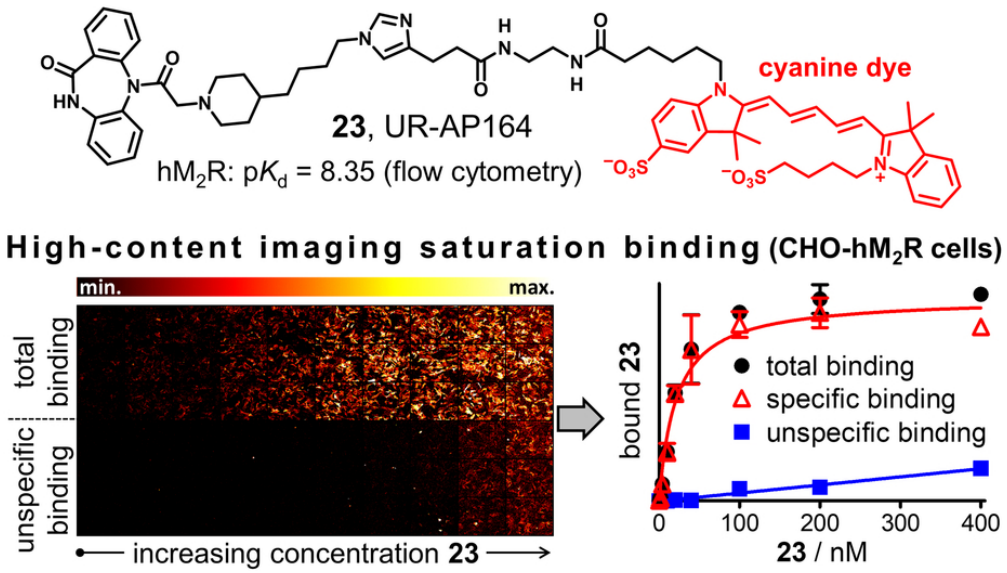

Note: for Table of Contents only

78x44mm (300 x 300 DPI)